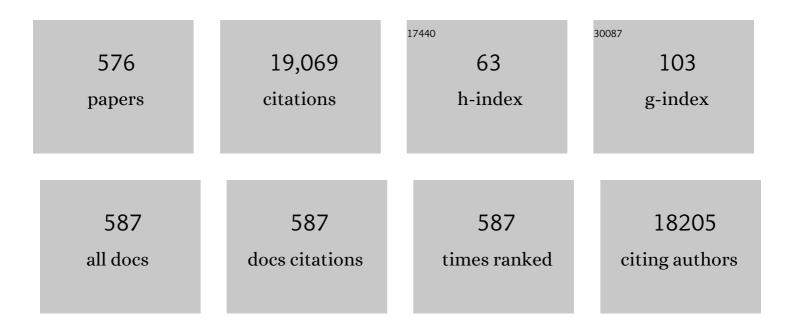
List of Publications by Year in descending order

Source: https://exaly.com/author-pdf/4436/publications.pdf Version: 2024-02-01



#	Article	IF	CITATIONS
1	Deep High-Resolution Representation Learning for Visual Recognition. IEEE Transactions on Pattern Analysis and Machine Intelligence, 2021, 43, 3349-3364.	13.9	1,553
2	STING directly activates autophagy to tune the innate immune response. Cell Death and Differentiation, 2019, 26, 1735-1749.	11.2	247
3	A Convolutional Neural Network Approach for Post-Processing in HEVC Intra Coding. Lecture Notes in Computer Science, 2017, , 28-39.	1.3	211
4	Autophagy protects auditory hair cells against neomycin-induced damage. Autophagy, 2017, 13, 1884-1904.	9.1	195
5	Postcollisional potassic and ultrapotassic rocks in southern Tibet: Mantle and crustal origins in response to India–Asia collision and convergence. Geochimica Et Cosmochimica Acta, 2014, 143, 207-231.	3.9	187
6	Selective photoelectrochemical oxidation of glycerol to high value-added dihydroxyacetone. Nature Communications, 2019, 10, 1779.	12.8	185
7	Novel conductive binder for high-performance silicon anodes in lithium ion batteries. Nano Energy, 2017, 36, 206-212.	16.0	178
8	Nobleâ€Metalâ€Free Janusâ€like Structures by Cation Exchange for Zâ€Scheme Photocatalytic Water Splitting under Broadband Light Irradiation. Angewandte Chemie - International Edition, 2017, 56, 4206-4210.	13.8	166
9	Hypoxic mitophagy regulates mitochondrial quality and platelet activation and determines severity of I/R heart injury. ELife, 2016, 5, .	6.0	158
10	Nanowire Photoelectrochemistry. Chemical Reviews, 2019, 119, 9221-9259.	47.7	158
11	Arabidopsis PHL2 and PHR1 Act Redundantly as the Key Components of the Central Regulatory System Controlling Transcriptional Responses to Phosphate Starvation. Plant Physiology, 2016, 170, 499-514.	4.8	155
12	Surface Reconstruction and Phase Transition on Vanadium–Cobalt–Iron Trimetal Nitrides to Form Active Oxyhydroxide for Enhanced Electrocatalytic Water Oxidation. Advanced Energy Materials, 2020, 10, 2002464.	19.5	155
13	Metastasis-associated miR-23a from nasopharyngeal carcinoma-derived exosomes mediates angiogenesis by repressing a novel target gene TSGA10. Oncogene, 2018, 37, 2873-2889.	5.9	154
14	Image Compression With Edge-Based Inpainting. IEEE Transactions on Circuits and Systems for Video Technology, 2007, 17, 1273-1287.	8.3	152
15	Functionalization of graphene materials by heteroatom-doping for energy conversion and storage. Progress in Natural Science: Materials International, 2018, 28, 121-132.	4.4	148
16	The Big Five personality traits, Big Two metatraits and social media: A meta-analysis. Journal of Research in Personality, 2017, 70, 229-240.	1.7	144
17	Flt1 acts as a negative regulator of tip cell formation and branching morphogenesis in the zebrafish embryo. Development (Cambridge), 2011, 138, 2111-2120.	2.5	142
18	Northward subduction of Bangong–Nujiang Tethys: Insight from Late Jurassic intrusive rocks from Bangong Tso in western Tibet. Lithos, 2014, 205, 284-297.	1.4	140

#	Article	IF	CITATIONS
19	Facile Processing of Free-Standing Polyaniline/SWCNT Film as an Integrated Electrode for Flexible Supercapacitor Application. ACS Applied Materials & Interfaces, 2017, 9, 33791-33801.	8.0	139
20	Integration of Multiple Plasmonic and Co-Catalyst Nanostructures on TiO ₂ Nanosheets for Visible-Near-Infrared Photocatalytic Hydrogen Evolution. Small, 2016, 12, 1640-1648.	10.0	136
21	Deficiency of mitophagy receptor FUNDC1 impairs mitochondrial quality and aggravates dietary-induced obesity and metabolic syndrome. Autophagy, 2019, 15, 1882-1898.	9.1	131
22	Pseudo-sequence-based light field image compression. , 2016, , .		130
23	A Meta-Analysis of Social Networking Online and Social Capital. Review of General Psychology, 2016, 20, 369-391.	3.2	129
24	Large-area synthesis of monolayer WSe ₂ on a SiO ₂ /Si substrate and its device applications. Nanoscale, 2015, 7, 4193-4198.	5.6	128
25	Social networking online and personality of self-worth: A meta-analysis. Journal of Research in Personality, 2016, 64, 79-89.	1.7	128
26	Combustion chemistry and flame structure of furan group biofuels using molecular-beam mass spectrometry and gas chromatography – Part III: 2,5-Dimethylfuran. Combustion and Flame, 2014, 161, 780-797.	5.2	127
27	Multi-Scale Triplet CNN for Person Re-Identification. , 2016, , .		124
28	Ultrathin-metal-film-based transparent electrodes with relative transmittance surpassing 100%. Nature Communications, 2020, 11, 3367.	12.8	123
29	Enhanced full-spectrum water splitting by confining plasmonic Au nanoparticles in N-doped TiO2 bowl nanoarrays. Nano Energy, 2016, 24, 87-93.	16.0	118
30	Combustion chemistry and flame structure of furan group biofuels using molecular-beam mass spectrometry and gas chromatography – Part I: Furan. Combustion and Flame, 2014, 161, 748-765.	5.2	117
31	Self-disclosure on social networking sites, positive feedback, and social capital among Chinese college students. Computers in Human Behavior, 2014, 38, 213-219.	8.5	116
32	Combustion chemistry and flame structure of furan group biofuels using molecular-beam mass spectrometry and gas chromatography – Part II: 2-Methylfuran. Combustion and Flame, 2014, 161, 766-779.	5.2	110
33	Dominant-Current Deep Learning Scheme for Electrical Impedance Tomography. IEEE Transactions on Biomedical Engineering, 2019, 66, 2546-2555.	4.2	109
34	Origin of the ca. 90 Ma magnesia-rich volcanic rocks in SE Nyima, central Tibet: Products of lithospheric delamination beneath the Lhasa-Qiangtang collision zone. Lithos, 2014, 198-199, 24-37.	1.4	106
35	Convolutional Neural Network-Based Block Up-Sampling for Intra Frame Coding. IEEE Transactions on Circuits and Systems for Video Technology, 2018, 28, 2316-2330.	8.3	103
36	Pd-Ag alloy hollow nanostructures with interatomic charge polarization for enhanced electrocatalytic formic acid oxidation. Nano Research, 2016, 9, 1590-1599.	10.4	102

#	Article	IF	CITATIONS
37	Motives Matter: Motives for Playing Pokémon Go and Implications for Well-Being. Cyberpsychology, Behavior, and Social Networking, 2017, 20, 52-57.	3.9	100
38	The Nature of Photocatalytic "Water Splitting―on Silicon Nanowires. Angewandte Chemie - International Edition, 2015, 54, 2980-2985.	13.8	97
39	A compact Cas9 ortholog from Staphylococcus Auricularis (SauriCas9) expands the DNA targeting scope. PLoS Biology, 2020, 18, e3000686.	5.6	96
40	Flame structure and kinetic studies of carbon dioxide-diluted dimethyl ether flames at reduced and elevated pressures. Combustion and Flame, 2013, 160, 2654-2668.	5.2	95
41	Hypoxia-Induced Matrix Metalloproteinase-13 Expression in Exosomes from Nasopharyngeal Carcinoma Enhances Metastases. Cell Death and Disease, 2018, 9, 382.	6.3	92
42	Reconstruction of soot temperature and volume fraction profiles of an asymmetric flame using stereoscopic tomography. Combustion and Flame, 2009, 156, 565-573.	5.2	91
43	An episomal vector-based CRISPR/Cas9 system for highly efficient gene knockout in human pluripotent stem cells. Scientific Reports, 2017, 7, 2320.	3.3	91
44	Chemical Approaches to Carbonâ€Based Metalâ€Free Catalysts. Advanced Materials, 2019, 31, e1804863.	21.0	90
45	Strong Metal–Support Interaction Boosts Activity, Selectivity, and Stability in Electrosynthesis of H ₂ O ₂ . Journal of the American Chemical Society, 2022, 144, 2255-2263.	13.7	90
46	Geochronology and geochemistry of the Early Jurassic Yeba Formation volcanic rocks in southern Tibet: Initiation of back-arc rifting and crustal accretion in the southern Lhasa Terrane. Lithos, 2017, 278-281, 477-490.	1.4	89
47	A meta-analysis of the relationship of academic performance and Social Network Site use among adolescents and young adults. Computers in Human Behavior, 2017, 77, 148-157.	8.5	89
48	Branched comb-shaped poly(arylene ether sulfone)s containing flexible alkyl imidazolium side chains as anion exchange membranes. Journal of Materials Chemistry A, 2018, 6, 10879-10890.	10.3	88
49	Learning a Convolutional Neural Network for Image Compact-Resolution. IEEE Transactions on Image Processing, 2019, 28, 1092-1107.	9.8	87
50	Zircon xenocrysts in Tibetan ultrapotassic magmas: Imaging the deep crust through time. Geology, 2014, 42, 43-46.	4.4	85
51	Preparation of porous MoO ₂ @C nano-octahedrons from a polyoxometalate-based metal–organic framework for highly reversible lithium storage. Journal of Materials Chemistry A, 2016, 4, 12434-12441.	10.3	83
52	Identifying mantle carbonatite metasomatism through Os–Sr–Mg isotopes in Tibetan ultrapotassic rocks. Earth and Planetary Science Letters, 2015, 430, 458-469.	4.4	82
53	Photoelectrocatalytic degradation of methylene blue using F doped TiO2 photoelectrode under visible light irradiation. Chemosphere, 2017, 185, 574-581.	8.2	82
54	Deep Learning-Based Video Coding. ACM Computing Surveys, 2021, 53, 1-35.	23.0	78

#	Article	IF	CITATIONS
55	Effects of butanol isomers additions on soot nanostructure and reactivity in normal and inverse ethylene diffusion flames. Fuel, 2017, 205, 109-129.	6.4	77
56	Facile synthesis of three-dimensional hollow porous carbon doped polymeric carbon nitride with highly efficient photocatalytic performance. Chemical Engineering Journal, 2022, 438, 135623.	12.7	74
57	An Efficient Four-Parameter Affine Motion Model for Video Coding. IEEE Transactions on Circuits and Systems for Video Technology, 2018, 28, 1934-1948.	8.3	73
58	Genetic Dissection of Fe-Dependent Signaling in Root Developmental Responses to Phosphate Deficiency. Plant Physiology, 2019, 179, 300-316.	4.8	72
59	Self-templating synthesis of heteroatom-doped large-scalable carbon anodes for high-performance lithium-ion batteries. Inorganic Chemistry Frontiers, 2022, 9, 1058-1069.	6.0	72
60	Deep Learning-Based Classification of Liver Cancer Histopathology Images Using Only Global Labels. IEEE Journal of Biomedical and Health Informatics, 2020, 24, 1643-1651.	6.3	71
61	Nitrogen-rich holey graphene for efficient oxygen reduction reaction. Carbon, 2020, 162, 66-73.	10.3	71
62	A Parametric Level Set Method for Electrical Impedance Tomography. IEEE Transactions on Medical Imaging, 2018, 37, 451-460.	8.9	70
63	Dimethyl Carbonate as a Promising Oxygenated Fuel for Combustion: A Review. Energies, 2018, 11, 1552.	3.1	70
64	Enhanced visible light photoelectrocatalytic degradation of tetracycline hydrochloride by I and P co-doped TiO2 photoelectrode. Journal of Hazardous Materials, 2021, 406, 124309.	12.4	70
65	A computer vision-based method for spatial-temporal action recognition of tail-biting behaviour in group-housed pigs. Biosystems Engineering, 2020, 195, 27-41.	4.3	70
66	MicroRNA-10a/10b represses a novel target gene mib1 to regulate angiogenesis. Cardiovascular Research, 2016, 110, 140-150.	3.8	69
67	Improving triplet-wise training of convolutional neural network for vehicle re-identification. , 2017, ,		69
68	Nitrogen, Sulfur Co-Doped Hierarchically Porous Carbon as a Metal-Free Electrocatalyst for Oxygen Reduction and Carbon Dioxide Reduction Reaction. ACS Applied Materials & Interfaces, 2020, 12, 44578-44587.	8.0	69
69	Dark-field microscopic image stitching method for surface defects evaluation of large fine optics. Optics Express, 2013, 21, 5974.	3.4	68
70	Highly improved electrocatalytic activity of NiSx: Effects of Cr-doping and phase transition. Applied Catalysis B: Environmental, 2020, 267, 118721.	20.2	68
71	Differential Gene Expression Profiling and Biological Process Analysis in Proximal Nerve Segments after Sciatic Nerve Transection. PLoS ONE, 2013, 8, e57000.	2.5	67
72	Nanostructure evolution and reactivity of nascent soot from inverse diffusion flames in CO2, N2, and He atmospheres. Carbon, 2018, 139, 172-180.	10.3	66

#	Article	IF	CITATIONS
73	Practical methods for retrace error correction in nonnull aspheric testing. Optics Express, 2009, 17, 7025.	3.4	64
74	Flexible Nearâ€Infrared Photovoltaic Devices Based on Plasmonic Hotâ€Electron Injection into Silicon Nanowire Arrays. Angewandte Chemie - International Edition, 2016, 55, 4577-4581.	13.8	64
75	Convolutional Neural Network-Based Fractional-Pixel Motion Compensation. IEEE Transactions on Circuits and Systems for Video Technology, 2019, 29, 840-853.	8.3	64
76	Silicon nanostructures for solar-driven catalytic applications. Nano Today, 2017, 17, 96-116.	11.9	63
77	Pseudo-Sequence-Based 2-D Hierarchical Coding Structure for Light-Field Image Compression. IEEE Journal on Selected Topics in Signal Processing, 2017, 11, 1107-1119.	10.8	63
78	Prescribed Performance Model-Free Adaptive Integral Sliding Mode Control for Discrete-Time Nonlinear Systems. IEEE Transactions on Neural Networks and Learning Systems, 2019, 30, 2222-2230.	11.3	63
79	miR-30a Regulates Endothelial Tip Cell Formation and Arteriolar Branching. Hypertension, 2013, 62, 592-598.	2.7	62
80	Nobleâ€Metalâ€Free Janusâ€like Structures by Cation Exchange for Zâ€Scheme Photocatalytic Water Splitting under Broadband Light Irradiation. Angewandte Chemie, 2017, 129, 4270-4274.	2.0	62
81	Enhanced visible light photoelectrocatalytic degradation of organic contaminants by F and Sn co-doped TiO2 photoelectrode. Chemical Engineering Journal, 2018, 344, 332-341.	12.7	62
82	Carbon nanotubes with fluorine-rich surface as metal-free electrocatalyst for effective synthesis of urea from nitrate and CO2. Applied Catalysis B: Environmental, 2022, 316, 121618.	20.2	62
83	End-to-End Optimized Versatile Image Compression With Wavelet-Like Transform. IEEE Transactions on Pattern Analysis and Machine Intelligence, 2022, 44, 1247-1263.	13.9	61
84	Boron, nitrogen co-doped carbon with abundant mesopores for efficient CO2 electroreduction. Applied Catalysis B: Environmental, 2021, 298, 120543.	20.2	61
85	Topological Defectâ€Rich Carbon as a Metalâ€Free Cathode Catalyst for Highâ€Performance Liâ€CO ₂ Batteries. Advanced Energy Materials, 2021, 11, 2101390.	19.5	60
86	Data-Driven Adaptive Sliding Mode Control of Nonlinear Discrete-Time Systems With Prescribed Performance. IEEE Transactions on Systems, Man, and Cybernetics: Systems, 2019, 49, 2598-2604.	9.3	59
87	Microscopic scattering imaging measurement and digital evaluation system of defects for fine optical surface. Optics Communications, 2007, 278, 240-246.	2.1	58
88	Practical phase unwrapping of interferometric fringes based on unscented Kalman filter technique. Optics Express, 2015, 23, 32337.	3.4	58
89	Media Niche of Electronic Communication Channels in Friendship: A Meta-Analysis. Journal of Computer-Mediated Communication, 2016, 21, 451-466.	3.3	58
90	Synthesis and properties of highly branched polybenzimidazoles as proton exchange membranes for high-temperature fuel cells. Journal of Materials Chemistry C, 2016, 4, 4814-4821.	5.5	58

#	Article	IF	CITATIONS
91	Assessing the depolarization capabilities of nonspherical particles in a super-ellipsoidal shape space. Optics Express, 2018, 26, 1726.	3.4	57
92	A Parametric Level Set-Based Approach to Difference Imaging in Electrical Impedance Tomography. IEEE Transactions on Medical Imaging, 2019, 38, 145-155.	8.9	57
93	Nonlinear Difference Imaging Approach to Three-Dimensional Electrical Impedance Tomography in the Presence of Geometric Modeling Errors. IEEE Transactions on Biomedical Engineering, 2016, 63, 1956-1965.	4.2	56
94	Experimental reconstructions of flame temperature distributions in laboratory-scale and large-scale pulverized-coal fired furnaces by inverse radiation analysis. Fuel, 2012, 93, 397-403.	6.4	55
95	NiFe Hydroxide Lattice Tensile Strain: Enhancement of Adsorption of Oxygenated Intermediates for Efficient Water Oxidation Catalysis. Angewandte Chemie, 2019, 131, 746-750.	2.0	55
96	One-for-All: Grouped Variation Network-Based Fractional Interpolation in Video Coding. IEEE Transactions on Image Processing, 2019, 28, 2140-2151.	9.8	55
97	Birth cohort changes of Chinese adolescents' anxiety: A cross-temporal meta-analysis, 1992–2005. Personality and Individual Differences, 2010, 48, 208-212.	2.9	54
98	Relative roles of spatial factors, environmental filtering and biotic interactions in fine-scale structuring of a soil mite community. Soil Biology and Biochemistry, 2014, 79, 68-77.	8.8	54
99	Solar energy conversion with tunable plasmonic nanostructures for thermoelectric devices. Nanoscale, 2012, 4, 4416.	5.6	53
100	NgAgo-based fabp11a gene knockdown causes eye developmental defects in zebrafish. Cell Research, 2016, 26, 1349-1352.	12.0	53
101	pH-sensitive zwitterionic coating of gold nanocages improves tumor targeting and photothermal treatment efficacy. Nano Research, 2018, 11, 3193-3204.	10.4	53
102	Retrieval and analysis of a polarized high-spectral-resolution lidar for profiling aerosol optical properties. Optics Express, 2013, 21, 13084.	3.4	52
103	Breaking the symmetry: Gradient in NiFe layered double hydroxide nanoarrays for efficient oxygen evolution. Nano Energy, 2019, 60, 661-666.	16.0	52
104	3D interconnected porous g-C3N4 hybridized with Fe2O3 quantum dots for enhanced photo-Fenton performance. Applied Surface Science, 2021, 555, 149677.	6.1	52
105	A nonlinear approach to difference imaging in EIT; assessment of the robustness in the presence of modelling errors. Inverse Problems, 2015, 31, 035012.	2.0	51
106	Plasmonic Coupling Architectures for Enhanced Photocatalysis. Advanced Materials, 2021, 33, e2005738.	21.0	51
107	Single copper sites dispersed on hierarchically porous carbon for improving oxygen reduction reaction towards zinc-air battery. Nano Research, 2021, 14, 998-1003.	10.4	50
108	Laminar flame propagation and ignition properties of premixed iso-octane/air with hydrogen addition. Fuel, 2015, 158, 443-450.	6.4	49

#	Article	IF	CITATIONS
109	A Statistical Shape-Constrained Reconstruction Framework for Electrical Impedance Tomography. IEEE Transactions on Medical Imaging, 2019, 38, 2400-2410.	8.9	49
110	Simultaneously Engineering the Coordination Environment and Pore Architecture of Metal–Organic Frameworkâ€Derived Singleâ€Atomic Iron Catalysts for Ultraefficient Oxygen Reduction. Small, 2021, 17, e2102425.	10.0	49
111	Optically Active Particles of Chiral Polymers. Macromolecular Rapid Communications, 2013, 34, 1426-1445.	3.9	48
112	Effects of an electrospun fluorinated poly(ether ether ketone) separator on the enhanced safety and electrochemical properties of lithium ion batteries. Electrochimica Acta, 2018, 290, 150-164.	5.2	48
113	Detection of aggressive behaviours in pigs using a RealSence depth sensor. Computers and Electronics in Agriculture, 2019, 166, 105003.	7.7	48
114	E2I: Generative Inpainting From Edge to Image. IEEE Transactions on Circuits and Systems for Video Technology, 2021, 31, 1308-1322.	8.3	48
115	Effects of alkali and alkaline earth metal species on the combustion characteristics of single particles from pine sawdust and bituminous coal. Bioresource Technology, 2018, 268, 278-285.	9.6	47
116	Effects of water addition on soot properties in ethylene inverse diffusion flames. Fuel, 2019, 247, 187-197.	6.4	47
117	N, P, and S tri-doped holey carbon as an efficient electrocatalyst for oxygen reduction in whole pH range for fuel cell and zinc-air batteries. Carbon, 2021, 179, 365-376.	10.3	47
118	3D interconnected g-C3N4 hybridized with 2D Ti3C2 MXene nanosheets for enhancing visible light photocatalytic hydrogen evolution and dye contaminant elimination. Applied Surface Science, 2022, 579, 152180.	6.1	47
119	A novel fuzzy classification entropy approach to image thresholding. Pattern Recognition Letters, 2006, 27, 1968-1975.	4.2	46
120	yap is required for the development of brain, eyes, and neural crest in zebrafish. Biochemical and Biophysical Research Communications, 2009, 384, 114-119.	2.1	46
121	Improvement in the mechanical properties, proton conductivity, and methanol resistance of highly branched sulfonated poly(arylene ether)/graphene oxide grafted with flexible alkylsulfonated side chains nanocomposite membranes. Journal of Power Sources, 2018, 378, 451-459.	7.8	46
122	A Three-Dimensional Culture System with Matrigel Promotes Purified Spiral Ganglion Neuron Survival and Function In Vitro. Molecular Neurobiology, 2018, 55, 2070-2084.	4.0	46
123	Convolutional Neural Network-Based Block Up-Sampling for HEVC. IEEE Transactions on Circuits and Systems for Video Technology, 2019, 29, 3701-3715.	8.3	46
124	A convolutional neural network approach for half-pel interpolation in video coding. , 2017, , .		45
125	Efficient inverse radiation analysis of temperature distribution in participating medium based on backward Monte Carlo method. Journal of Quantitative Spectroscopy and Radiative Transfer, 2008, 109, 2171-2181.	2.3	44
126	Simultaneous measurements of two-dimensional temperature and particle concentration distribution from the image of the pulverized-coal flame. Fuel, 2010, 89, 202-211.	6.4	44

#	Article	IF	CITATIONS
127	Nonmuscle myosin II-B (myh10) expression analysis during zebrafish embryonic development. Gene Expression Patterns, 2013, 13, 265-270.	0.8	44
128	Detailed influences of chemical effects of hydrogen as fuel additive on methane flame. International Journal of Hydrogen Energy, 2015, 40, 3777-3788.	7.1	44
129	Effects of branching structures on the properties of phosphoric acid-doped polybenzimidazole as a membrane material for high-temperature proton exchange membrane fuel cells. International Journal of Hydrogen Energy, 2018, 43, 16694-16703.	7.1	44
130	A Moving Morphable Components Based Shape Reconstruction Framework for Electrical Impedance Tomography. IEEE Transactions on Medical Imaging, 2019, 38, 2937-2948.	8.9	44
131	Kinetic analysis of the chemical effects of hydrogen addition on dimethyl ether flames. International Journal of Hydrogen Energy, 2014, 39, 13014-13019.	7.1	43
132	Circuits and Systems Issues in Power Electronics Penetrated Power Grid. IEEE Open Journal of Circuits and Systems, 2020, 1, 140-156.	1.9	43
133	Estimation of conductivity changes in a region of interest with electrical impedance tomography. Inverse Problems and Imaging, 2015, 9, 211-229.	1.1	43
134	Defect Engineering in Photocatalytic Methane Conversion. Small Structures, 2022, 3, 2100147.	12.0	43
135	Textile-based moisture power generator with dual asymmetric structure and high flexibility for wearable applications. Nano Energy, 2022, 95, 107017.	16.0	43
136	Peroxymonosulfate activation by Co3O4/SnO2 for efficient degradation of ofloxacin under visible light. Journal of Colloid and Interface Science, 2022, 615, 650-662.	9.4	43
137	Geometrically Deformed Iron-Based Single-Atom Catalysts for High-Performance Acidic Proton Exchange Membrane Fuel Cells. ACS Catalysis, 2022, 12, 5397-5406.	11.2	43
138	Insm1a Regulates Motor Neuron Development in Zebrafish. Frontiers in Molecular Neuroscience, 2017, 10, 274.	2.9	42
139	iWave: CNN-Based Wavelet-Like Transform for Image Compression. IEEE Transactions on Multimedia, 2020, 22, 1667-1679.	7.2	42
140	Self-Healing Solid Polymer Electrolyte with High Ion Conductivity and Super Stretchability for All-Solid Zinc-Ion Batteries. ACS Applied Materials & amp; Interfaces, 2021, 13, 36320-36329.	8.0	42
141	Site-density engineering of single-atomic iron catalysts for high-performance proton exchange membrane fuel cells. Applied Catalysis B: Environmental, 2022, 302, 120860.	20.2	42
142	Inpainting with image patches for compression. Journal of Visual Communication and Image Representation, 2012, 23, 100-113.	2.8	41
143	A Parametric Level set Method for Imaging Multiphase Conductivity Using Electrical Impedance Tomography. IEEE Transactions on Computational Imaging, 2018, 4, 552-561.	4.4	41
144	B-Spline-Based Sharp Feature Preserving Shape Reconstruction Approach for Electrical Impedance Tomography. IEEE Transactions on Medical Imaging, 2019, 38, 2533-2544.	8.9	41

#	Article	IF	CITATIONS
145	The <i>slc4a2b</i> gene is required for hair cell development in zebrafish. Aging, 2020, 12, 18804-18821.	3.1	41
146	Real time diagnosis of transient pulse laser with high repetition by radial shearing interferometer. Applied Optics, 2007, 46, 8305.	2.1	40
147	Birth Cohort and Age Changes in the Selfâ€Esteem of Chinese Adolescents: A Crossâ€Temporal Metaâ€Analysis, 1996–2009. Journal of Research on Adolescence, 2015, 25, 366-376.	3.7	40
148	Quadriwave lateral shearing interferometer based on a randomly encoded hybrid grating. Optics Letters, 2015, 40, 2245.	3.3	40
149	Minimizing cross-axis sensitivity in grating-based optomechanical accelerometers. Optics Express, 2016, 24, 9094.	3.4	40
150	The structural development of primary cultured hippocampal neurons on a graphene substrate. Colloids and Surfaces B: Biointerfaces, 2016, 146, 442-451.	5.0	40
151	A Conductive Binder for High-Performance Sn Electrodes in Lithium-Ion Batteries. ACS Applied Materials & Interfaces, 2018, 10, 1672-1677.	8.0	40
152	Transparent Perfect Microwave Absorber Employing Asymmetric Resonance Cavity. Advanced Science, 2019, 6, 1901320.	11.2	40
153	Nonstationary Shape Estimation in Electrical Impedance Tomography Using a Parametric Level Set-Based Extended Kalman Filter Approach. IEEE Transactions on Instrumentation and Measurement, 2020, 69, 1894-1907.	4.7	40
154	Zero-Shot Depth Estimation From Light Field Using A Convolutional Neural Network. IEEE Transactions on Computational Imaging, 2020, 6, 682-696.	4.4	40
155	Deep Adversarial Data Augmentation for Extremely Low Data Regimes. IEEE Transactions on Circuits and Systems for Video Technology, 2021, 31, 15-28.	8.3	40
156	Noncontact temperature measurement by means of CCD cameras in a participating medium. Optics Letters, 2008, 33, 422.	3.3	39
157	System analysis of a tilted field-widened Michelson interferometer for high spectral resolution lidar. Optics Express, 2012, 20, 1406.	3.4	39
158	Kinesinâ€12 influences axonal growth during zebrafish neural development. Cytoskeleton, 2014, 71, 555-563.	2.0	39
159	Automated discrimination between digs and dust particles on optical surfaces with dark-field scattering microscopy. Applied Optics, 2014, 53, 5131.	1.8	39
160	Defects evaluation system for spherical optical surfaces based on microscopic scattering dark-field imaging method. Applied Optics, 2016, 55, 6162.	2.1	38
161	Leucogranites in Lhozag, southern Tibet: Implications for the tectonic evolution of the eastern Himalaya. Lithos, 2017, 294-295, 246-262.	1.4	38
162	Effects of Flame Configuration and Soot Aging on Soot Nanostructure and Reactivity in <i>n</i> Butanol-Doped Ethylene Diffusion Flames. Energy & Fuels, 2018, 32, 607-624.	5.1	38

#	Article	IF	CITATIONS
163	Partition-Aware Adaptive Switching Neural Networks for Post-Processing in HEVC. IEEE Transactions on Multimedia, 2020, 22, 2749-2763.	7.2	38
164	Fabricating I doped TiO2 photoelectrode for the degradation of diclofenac: Performance and mechanism study. Chemical Engineering Journal, 2019, 369, 968-978.	12.7	37
165	Non-null annular subaperture stitching interferometry for steep aspheric measurement. Applied Optics, 2014, 53, 5755.	1.8	36
166	Reverse optimization reconstruction of aspheric figure error in a non-null interferometer. Applied Optics, 2014, 53, 5538.	1.8	36
167	CYP6B6 is involved in esfenvalerate detoxification in the polyphagous lepidopteran pest, Helicoverpa armigera. Pesticide Biochemistry and Physiology, 2017, 138, 51-56.	3.6	36
168	An Intrinsically Disordered Peptide-Peptide Stapler for Highly Efficient Protein Ligation Both <i>in Vivo</i> and <i>in Vitro</i> . Journal of the American Chemical Society, 2018, 140, 17474-17483.	13.7	36
169	Synthesis and properties of highly branched sulfonated poly(arylene ether)s with flexible alkylsulfonated side chains as proton exchange membranes. Journal of Materials Chemistry C, 2016, 4, 1326-1335.	5.5	35
170	Block-Composed Background Reference for High Efficiency Video Coding. IEEE Transactions on Circuits and Systems for Video Technology, 2017, 27, 2639-2651.	8.3	35
171	Combustion Characteristics of Single Particles from Bituminous Coal and Pine Sawdust in O2/N2, O2/CO2, and O2/H2O Atmospheres. Energies, 2017, 10, 1695.	3.1	35
172	Inverse radiation analysis for simultaneous reconstruction of temperature and volume fraction fields of soot and metal-oxide nanoparticles in a nanofluid fuel sooting flame. International Journal of Heat and Mass Transfer, 2018, 118, 1080-1089.	4.8	35
173	Mesoporous implantable Pt/SrTiO3:C,N nanocuboids delivering enhanced photocatalytic H2-production activity via plasmon-induced interfacial electron transfer. Applied Catalysis B: Environmental, 2018, 236, 338-347.	20.2	35
174	Feature extraction of rotor fault based on EEMD and curve code. Measurement: Journal of the International Measurement Confederation, 2019, 135, 712-724.	5.0	35
175	Oribatid mites of China: a review of progress, with a checklist . Zoosymposia, 2010, 4, 186-224.	0.3	35
176	The study of co-combustion characteristics of coal and microalgae by single particle combustion and TGA methods. Journal of the Energy Institute, 2020, 93, 508-517.	5.3	34
177	A Comprehensive Benchmark for Single Image Compression Artifact Reduction. IEEE Transactions on Image Processing, 2020, 29, 7845-7860.	9.8	34
178	Catalogue of ptyctimous mites (Acari, Oribatida) of the world. Zootaxa, 2018, 4393, 1.	0.5	33
179	Planar Metasurfaces Enable Highâ€Efficiency Colored Perovskite Solar Cells. Advanced Science, 2018, 5, 1800836.	11.2	33
180	Lidar Remote Sensing of Seawater Optical Properties: Experiment and Monte Carlo Simulation. IEEE Transactions on Geoscience and Remote Sensing, 2019, 57, 9489-9498.	6.3	33

#	Article	IF	CITATIONS
181	Magnetic Fe ₃ O ₄ â€PSâ€Polyacetylene Composite Microspheres Showing Chirality Derived From Helical Substituted Polyacetylene. Macromolecular Rapid Communications, 2012, 33, 672-677.	3.9	32
182	Nanostructure and Oxidation Reactivity of Nascent Soot Particles in Ethylene/Pentanol Flames. Energies, 2017, 10, 122.	3.1	32
183	Cascading Failure of Cyber-Coupled Power Systems Considering Interactions Between Attack and Defense. IEEE Transactions on Circuits and Systems I: Regular Papers, 2019, 66, 4323-4336.	5.4	32
184	A facile approach to high-performance trifunctional electrocatalysts by substrate-enhanced electroless deposition of Pt/NiO/Ni on carbon nanotubes. Nanoscale, 2020, 12, 14615-14625.	5.6	32
185	Stability analysis of hydropower units under full operating conditions considering turbine nonlinearity. Renewable Energy, 2020, 154, 723-742.	8.9	32
186	Learning and Fusing Multiple User Interest Representations for Micro-Video and Movie Recommendations. IEEE Transactions on Multimedia, 2021, 23, 484-496.	7.2	32
187	Practical and accurate method for aspheric misalignment aberrations calibration in non-null interferometric testing. Applied Optics, 2013, 52, 8501.	1.8	31
188	Fe ₂ O ₃ , a cost effective and environmentally friendly catalyst for the generation of NH ₃ – a future fuel – using a new Al ₂ O ₃ -looping based technology. Chemical Communications, 2017, 53, 10664-10667.	4.1	31
189	Fast Image Super-Resolution via Local Adaptive Gradient Field Sharpening Transform. IEEE Transactions on Image Processing, 2018, 27, 1966-1980.	9.8	31
190	N-desorption or NH3 generation of TiO2-loaded Al-based nitrogen carrier during chemical looping ammonia generation technology. International Journal of Hydrogen Energy, 2018, 43, 16589-16597.	7.1	31
191	Dry Reforming of Shale Gas and Carbon Dioxide with Niâ€Ceâ€Al ₂ O ₃ Catalyst: Syngas Production Enhanced over Niâ€CeO _x Formation. ChemCatChem, 2018, 10, 4689-4698.	3.7	31
192	Deep Learning-Based Technology in Responses to the Joint Call for Proposals on Video Compression With Capability Beyond HEVC. IEEE Transactions on Circuits and Systems for Video Technology, 2020, 30, 1267-1280.	8.3	31
193	Effects of oxygenated biofuel additives on soot formation: A comprehensive review of laboratory-scale studies. Fuel, 2022, 313, 122635.	6.4	31
194	Synthesis and characterization of magnetic Fe3O4-silica-poly(γ-benzyl-l-glutamate) composite microspheres. Reactive and Functional Polymers, 2011, 71, 1040-1044.	4.1	30
195	Optically active, magnetic gels consisting of helical substituted polyacetylene and Fe3O4 nanoparticles: preparation and chiral recognition ability. Journal of Materials Chemistry C, 2013, 1, 8066.	5.5	30
196	<inline-formula> <tex-math notation="LaTeX">\$lambda\$</tex-math> </inline-formula> -Domain Rate Control Algorithm for HEVC Scalable Extension. IEEE Transactions on Multimedia, 2016, 18, 2023-2039.	7.2	30
197	Combustion of single particles from sewage sludge/pine sawdust and sewage sludge/bituminous coal under oxy-fuel conditions with steam addition. Waste Management, 2020, 101, 1-8.	7.4	30
198	Recent Advances in Porous Materials for Photocatalytic CO ₂ Reduction. Journal of Physical Chemistry Letters, 2022, 13, 1272-1282.	4.6	30

#	Article	IF	CITATIONS
199	Effects of spectral discrimination in high-spectral-resolution lidar on the retrieval errors for atmospheric aerosol optical properties. Applied Optics, 2014, 53, 4386.	1.8	29
200	Pd–Ag alloy nanocages: integration of Ag plasmonic properties with Pd active sites for light-driven catalytic hydrogenation. Journal of Materials Chemistry A, 2015, 3, 9390-9394.	10.3	29
201	Side-chain effects on the properties of highly branched imidazolium-functionalized copolymer anion exchange membranes. Applied Surface Science, 2019, 493, 1306-1316.	6.1	29
202	Light Field Super-Resolution By Jointly Exploiting Internal and External Similarities. IEEE Transactions on Circuits and Systems for Video Technology, 2020, 30, 2604-2616.	8.3	29
203	PLD-fabricated perovskite oxide nanofilm as efficient electrocatalyst with highly enhanced water oxidation performance. Applied Catalysis B: Environmental, 2020, 272, 119046.	20.2	29
204	Aspheric subaperture stitching based on system modeling. Optics Express, 2015, 23, 19176.	3.4	28
205	3D-hybrid material design with electron/lithium-ion dual-conductivity for high-performance Li-sulfur batteries. Journal of Power Sources, 2017, 340, 160-166.	7.8	28
206	Nonlinear modeling and multi-scale damping characteristics of hydro-turbine regulation systems under complex variable hydraulic and electrical network structures. Applied Energy, 2021, 293, 116949.	10.1	28
207	A hollow PdCuMoNiCo high-entropy alloy as an efficient bi-functional electrocatalyst for oxygen reduction and formic acid oxidation. Journal of Materials Chemistry A, 2022, 10, 14857-14865.	10.3	28
208	Edge-Oriented Uniform Intra Prediction. IEEE Transactions on Image Processing, 2008, 17, 1827-1836.	9.8	27
209	Field-widened Michelson interferometer for spectral discrimination in high-spectral-resolution lidar: theoretical framework. Optics Express, 2015, 23, 12117.	3.4	27
210	Effects of multi-orifice configurations of the quench plate on mixing characteristics of the quench zone in an RQL-TVC model. Experimental Thermal and Fluid Science, 2017, 83, 57-68.	2.7	27
211	The effects of specific surface area and ash on char gasification mechanisms in the mixture of H2O, CO2, H2 and CO. Fuel, 2017, 209, 109-116.	6.4	27
212	Highly Crystalline Mesoporous Silicon Spheres for Efficient Visible Photocatalytic Hydrogen Evolution. ChemNanoMat, 2017, 3, 22-26.	2.8	27
213	Design of iodine absorption cell for high-spectral-resolution lidar. Optics Express, 2017, 25, 15913.	3.4	27
214	Automatic estimation of dairy cattle body condition score from depth image using ensemble model. Biosystems Engineering, 2020, 194, 16-27.	4.3	27
215	Ensemble Learning-Based Rate-Distortion Optimization for End-to-End Image Compression. IEEE Transactions on Circuits and Systems for Video Technology, 2021, 31, 1193-1207.	8.3	27
216	Nuclear exosome HMGB3 secreted by nasopharyngeal carcinoma cells promotes tumour metastasis by inducing angiogenesis. Cell Death and Disease, 2021, 12, 554.	6.3	27

#	Article	IF	CITATIONS
217	Effects of swirling combustion on soot characteristics in 2,5-dimethylfuran/n-heptane diffusion flames. Applied Thermal Engineering, 2018, 139, 11-24.	6.0	26
218	Multi-phase flow monitoring with electrical impedance tomography using level set based method. Nuclear Engineering and Design, 2015, 289, 108-116.	1.7	25
219	The pyrolysis and gasification performances of waste textile under carbon dioxide atmosphere. Journal of Thermal Analysis and Calorimetry, 2017, 128, 581-591.	3.6	25
220	Soot reduction by addition of dimethyl carbonate in normal and inverse ethylene diffusion flames: Nanostructural evidence. Journal of Environmental Sciences, 2018, 72, 107-117.	6.1	25
221	Robust Deep Co-Saliency Detection With Group Semantic and Pyramid Attention. IEEE Transactions on Neural Networks and Learning Systems, 2020, 31, 1-11.	11.3	25
222	A Tutorial on Modeling and Analysis of Cascading Failure in Future Power Grids. IEEE Transactions on Circuits and Systems II: Express Briefs, 2021, 68, 49-55.	3.0	25
223	Neuron navigator 3a regulates liver organogenesis during zebrafish embryogenesis. Development (Cambridge), 2011, 138, 1935-1945.	2.5	24
224	Common-path and compact wavefront diagnosis system based on cross grating lateral shearing interferometer. Applied Optics, 2014, 53, 7144.	1.8	24
225	Cooperative Nanoparticle System for Photothermal Tumor Treatment without Skin Damage. ACS Applied Materials & Interfaces, 2016, 8, 2847-2856.	8.0	24
226	Insm1a Is Required for Zebrafish Posterior Lateral Line Development. Frontiers in Molecular Neuroscience, 2017, 10, 241.	2.9	24
227	Study of Sewage Sludge/Coal Co-Combustion by Thermogravimetric Analysis and Single Particle Co-Combustion Method. Energy & Fuels, 2018, 32, 6300-6308.	5.1	24
228	Highly branched poly(arylene ether)/surface functionalized fullereneâ€based composite membrane electrolyte for DMFC applications. International Journal of Energy Research, 2019, 43, 3756-3767.	4.5	24
229	Promising zirconia-mixed Al-based nitrogen carriers for chemical looping of NH3: Reduced NH3 decomposition and improved NH3 yield. Fuel, 2020, 264, 116821.	6.4	24
230	Damping characteristics analysis of hydropower units under full operating conditions and control parameters: Accurate quantitative evaluation based on refined models. Applied Energy, 2021, 292, 116881.	10.1	24
231	Hotspots of new species discovery: new mite species described during 2007 to 2012. Zootaxa, 2013, 3663, 1.	0.5	23
232	Combustion characteristics of primary reference fuels with hydrogen addition. International Journal of Hydrogen Energy, 2016, 41, 11471-11480.	7.1	23
233	Sub-nanometer planar solar absorber. Nano Energy, 2017, 34, 172-180.	16.0	23
234	Pseudo Sequence Based 2-D Hierarchical Coding Structure for Light-Field Image Compression. , 2017, , .		23

#	Article	IF	CITATIONS
235	Catalytic pyrolysis and gasification of waste textile under carbon dioxide atmosphere with composite Zn-Fe catalyst. Fuel Processing Technology, 2017, 166, 115-123.	7.2	23
236	A TBX5 3′UTR variant increases the risk of congenital heart disease in the Han Chinese population. Cell Discovery, 2017, 3, 17026.	6.7	23
237	Effects of hydrogen additions on premixed rich flames of four butanol isomers. International Journal of Hydrogen Energy, 2017, 42, 3833-3841.	7.1	23
238	MIB1 mutations reduce Notch signaling activation and contribute to congenital heart disease. Clinical Science, 2018, 132, 2483-2491.	4.3	23
239	Semi-Supervised Community Detection Based on Distance Dynamics. IEEE Access, 2018, 6, 37261-37271.	4.2	23
240	High-performance mesoporous (AlN/Al2O3) for enhanced NH3 yield during chemical looping ammonia generation technology. International Journal of Hydrogen Energy, 2020, 45, 9903-9913.	7.1	23
241	Emerging Stacked Photocatalyst Design Enables Spatially Separated Ni(OH) ₂ Redox Cocatalysts for Overall CO ₂ Reduction and H ₂ O Oxidation. Small, 2022, 18, e2104681.	10.0	23
242	Optically active helical polyacetylene/Fe ₃ O ₄ composite microspheres: prepared by precipitation polymerization and used for enantioselective crystallization. RSC Advances, 2014, 4, 63611-63619.	3.6	22
243	Vegfa signaling regulates diverse artery/vein formation in vertebrate vasculatures. Journal of Genetics and Genomics, 2017, 44, 483-492.	3.9	22
244	Kinetic analysis of ethanol and dimethyl ether flames with hydrogen addition. International Journal of Hydrogen Energy, 2017, 42, 3813-3823.	7.1	22
245	Effects of dimethyl ether addition on soot formation, evolution and characteristics in flame-wall interactions. Energy, 2018, 164, 642-654.	8.8	22
246	The Preparation, Characterization and Formation Mechanism of a Calcium Phosphate Conversion Coating on Magnesium Alloy AZ91D. Materials, 2018, 11, 908.	2.9	22
247	Multiple Features Fusion Attention Mechanism Enhanced Deep Knowledge Tracing for Student Performance Prediction. IEEE Access, 2020, 8, 194894-194903.	4.2	22
248	The effect of acetic acid and acetate on CO ₂ corrosion of carbon steel. Anti-Corrosion Methods and Materials, 2008, 55, 130-134.	1.5	21
249	The role of blood flow and microRNAs in blood vessel development. International Journal of Developmental Biology, 2011, 55, 419-429.	0.6	21
250	Interferometric filters for spectral discrimination in high-spectral-resolution lidar: performance comparisons between Fabry–Perot interferometer and field-widened Michelson interferometer. Applied Optics, 2013, 52, 7838.	1.8	21
251	Distortion correction in surface defects evaluating system of large fine optics. Optics Communications, 2014, 312, 110-116.	2.1	21
252	Chemical Effects of Carbon Dioxide Addition on Dimethyl Ether and Ethanol Flames: A Comparative Study. Energy & Fuels, 2015, 29, 3385-3393.	5.1	21

#	Article	IF	CITATIONS
253	Detection of trace levels of Pd2+ in pure water using a fluorescent probe assisted by surfactants. Sensors and Actuators B: Chemical, 2016, 237, 899-904.	7.8	21
254	A semianalytic Monte Carlo radiative transfer model for polarized oceanic lidar: Experiment-based comparisons and multiple scattering effects analyses. Journal of Quantitative Spectroscopy and Radiative Transfer, 2019, 237, 106638.	2.3	21
255	Comparative study on characteristics of soot from n-decane and RP-3 kerosene normal/inverse diffusion flames. Journal of the Energy Institute, 2020, 93, 62-75.	5.3	21
256	Semantics-to-Signal Scalable Image Compression with Learned Revertible Representations. International Journal of Computer Vision, 2021, 129, 2605-2621.	15.6	21
257	Social Diffusion Analysis With Common-Interest Model for Image Annotation. IEEE Transactions on Multimedia, 2016, 18, 687-701.	7.2	20
258	Image Denoising via Low Rank Regularization Exploiting Intra and Inter Patch Correlation. IEEE Transactions on Circuits and Systems for Video Technology, 2018, 28, 3321-3332.	8.3	20
259	Soot in flame-wall interactions: Views from nanostructure and reactivity. Fuel, 2018, 212, 117-131.	6.4	20
260	Deep Network-Based Frame Extrapolation With Reference Frame Alignment. IEEE Transactions on Circuits and Systems for Video Technology, 2021, 31, 1178-1192.	8.3	20
261	On the treatment of scattering for three-dimensional temperature distribution reconstruction accuracy in participating medium. International Journal of Heat and Mass Transfer, 2011, 54, 1684-1687.	4.8	19
262	General measurement of optical system aberrations with a continuously variable lateral shear ratio by a randomly encoded hybrid grating. Applied Optics, 2015, 54, 8913.	2.1	19
263	Nanoscale Characteristics and Reactivity of Nascent Soot from n-Heptane/2,5-Dimethylfuran Inverse Diffusion Flames with/without Magnetic Fields. Energies, 2018, 11, 1698.	3.1	19
264	Validation of the Analytical Model of Oceanic Lidar Returns: Comparisons with Monte Carlo Simulations and Experimental Results. Remote Sensing, 2019, 11, 1870.	4.0	19
265	Relationship between the effective attenuation coefficient of spaceborne lidar signal and the IOPs of seawater. Optics Express, 2018, 26, 30278.	3.4	19
266	Performance estimation of space-borne high-spectral-resolution lidar for cloud and aerosol optical properties at 532 nm. Optics Express, 2019, 27, A481.	3.4	19
267	Measurement of transient near-infrared laser pulse wavefront with high precision by radial shearing interferometer. Optics Communications, 2007, 275, 173-178.	2.1	18
268	On the treatment of non-optimal regularization parameter influence on temperature distribution reconstruction accuracy in participating medium. International Journal of Heat and Mass Transfer, 2012, 55, 1553-1560.	4.8	18
269	Characterization of NADPH–cytochrome P450 reductase gene from the cotton bollworm, Helicoverpa armigera. Gene, 2014, 545, 262-270.	2.2	18
270	Combretastatin A-4 efficiently inhibits angiogenesis and induces neuronal apoptosis in zebrafish. Scientific Reports, 2016, 6, 30189.	3.3	18

#	Article	lF	CITATIONS
271	Preparation and properties of highly branched sulfonated poly(arylene ether)/polyacrylonitrile composite materials as proton exchange membranes. Journal of Materials Science, 2016, 51, 7119-7129.	3.7	18
272	Recognizable or Not: Towards Image Semantic Quality Assessment for Compression. Sensing and Imaging, 2017, 18, 1.	1.5	18
273	Three-dimensional BiOI/TiO2 heterostructures with photocatalytic activity under visible light irradiation. Journal of Porous Materials, 2018, 25, 1805-1812.	2.6	18
274	Invertibility-Driven Interpolation Filter for Video Coding. IEEE Transactions on Image Processing, 2019, 28, 4912-4925.	9.8	18
275	Experimental study on soot formation, evolution and characteristics of diffusion ethylene/air flames in Ĩ^-shaped mesoscale combustors. Fuel, 2019, 241, 138-154.	6.4	18
276	Soot properties in ethylene inverse diffusion flames blended with different carbon chain length alcohols. Fuel, 2021, 287, 119520.	6.4	18
277	High-performance metal–iodine batteries enabled by a bifunctional dendrite-free Li–Na alloy anode. Journal of Materials Chemistry A, 2021, 9, 538-545.	10.3	18
278	Compressed-Encoding Particle Swarm Optimization with Fuzzy Learning for Large-Scale Feature Selection. Symmetry, 2022, 14, 1142.	2.2	18
279	Towards Annotating Media Contents through Social Diffusion Analysis. , 2012, , .		17
280	Off-axis cyclic radial shearing interferometer for measurement of centrally blocked transient wavefront. Optics Letters, 2013, 38, 2493.	3.3	17
281	Two new species of <i>Austrophthiracarus</i> (Acari: Oribatida: Phthiracaridae) from New Zealand. Zootaxa, 2013, 3682, 385-91.	0.5	17
282	Helix-sense-selective polymerization of achiral substituted acetylene in chiral micelles for preparing optically active polymer nanoparticles: Effects of chiral emulsifiers. Polymer, 2014, 55, 840-847.	3.8	17
283	Practical retrace error correction in non-null aspheric testing: A comparison. Optics Communications, 2017, 383, 378-385.	2.1	17
284	Direct simultaneous reconstruction for temperature and concentration profiles of soot and metal-oxide nanoparticles in nanofluid fuel flames by a CCD camera. International Journal of Heat and Mass Transfer, 2018, 124, 564-575.	4.8	17
285	Nanostructure and reactivity of carbon particles from co-pyrolysis of biodiesel surrogate methyl octanoate blended with <i>n</i> -butanol. Fullerenes Nanotubes and Carbon Nanostructures, 2018, 26, 278-290.	2.1	17
286	Cobalt/titanium nitride@N-doped carbon hybrids for enhanced electrocatalytic hydrogen evolution and supercapacitance. New Journal of Chemistry, 2019, 43, 14518-14526.	2.8	17
287	Large-scale production of holey carbon nanosheets implanted with atomically dispersed Fe sites for boosting oxygen reduction electrocatalysis. Nano Research, 2022, 15, 1926-1933.	10.4	17
288	Single-atom-based catalysts for photoelectrocatalysis: challenges and opportunities. Journal of Materials Chemistry A, 2022, 10, 5878-5888.	10.3	17

#	Article	IF	CITATIONS
289	Ildr1b is essential for semicircular canal development, migration of the posterior lateral line primordium and hearing ability in zebrafish: implications for a role in the recessive hearing impairment DFNB42. Human Molecular Genetics, 2014, 23, 6201-6211.	2.9	16
290	Determination of aspheric vertex radius of curvature in non-null interferometry. Applied Optics, 2015, 54, 2838.	1.8	16
291	The THO/TREX Complex Active in miRNA Biogenesis Negatively Regulates Root-Associated Acid Phosphatase Activity Induced by Phosphate Starvation. Plant Physiology, 2016, 171, 2841-2853.	4.8	16
292	Simultaneous reconstruction of temperature and concentration profiles of soot and metal-oxide nanoparticles in asymmetric nanofluid fuel flames by inverse analysis. Journal of Quantitative Spectroscopy and Radiative Transfer, 2018, 219, 174-185.	2.3	16
293	Novel nanoscale control on soot formation by local CO2 micro-injection in ethylene inverse diffusion flames. Energy, 2019, 179, 697-708.	8.8	16
294	Block Copolymer Electrolytes with Excellent Properties in a Wide Temperature Range. ACS Applied Energy Materials, 2020, 3, 6536-6543.	5.1	16
295	Soot particles diagnostics in ethylene inverse diffusion flame blending with biodiesel surrogates of saturated methyl butyrate and unsaturated methyl crotonate. Fuel Processing Technology, 2020, 202, 106379.	7.2	16
296	A high-pressure artificial photosynthetic device: pumping carbon dioxide as well as achieving selectivity. Journal of Materials Chemistry A, 2021, 9, 3961-3967.	10.3	16
297	Nanostructured hexaazatrinaphthalene based polymers for advanced energy conversion and storage. Chemical Engineering Journal, 2022, 427, 130995.	12.7	16
298	Review of Plonaphacarus (Acari: Oribatida: Steganacaridae), with descriptions of eight new species from China. Zootaxa, 2011, 2739, .	0.5	16
299	Fault diagnosis of rotor using EMD thresholding-based de-noising combined with probabilistic neural network. Journal of Vibroengineering, 2017, 19, 5920-5931.	1.0	16
300	Effects of High Level of Penetration of Renewable Energy Sources on Cascading Failure of Modern Power Systems. IEEE Journal on Emerging and Selected Topics in Circuits and Systems, 2022, 12, 98-106.	3.6	16
301	Coal Char Gasification on a Circulating Fluidized Bed for Hydrogen Generation: Experiments and Simulation. Energy Technology, 2015, 3, 1059-1067.	3.8	15
302	The small-scale structure of a soil mite metacommunity. European Journal of Soil Biology, 2016, 74, 69-75.	3.2	15
303	Expression of SoxC Transcription Factors during Zebrafish Retinal and Optic Nerve Regeneration. Neuroscience Bulletin, 2017, 33, 53-61.	2.9	15
304	Retrieving the seawater volume scattering function at the 180° scattering angle with a high-spectral-resolution lidar. Optics Express, 2017, 25, 11813.	3.4	15
305	Thermodynamic and economic analyses of a novel coal pyrolysis–gasification–combustion staged conversion utilization polygeneration system. Asia-Pacific Journal of Chemical Engineering, 2018, 13, e2171.	1.5	15
306	Spherical Coordinates Transform-Based Motion Model for Panoramic Video Coding. IEEE Journal on Emerging and Selected Topics in Circuits and Systems, 2019, 9, 98-109.	3.6	15

#	Article	IF	CITATIONS
307	Clustered Regularly Interspaced Short Palindromic Repeats (CRISPR)/Cas9â€mediated <i>kif15</i> mutations accelerate axonal outgrowth during neuronal development and regeneration in zebrafish. Traffic, 2019, 20, 71-81.	2.7	15
308	Graph-Based Non-Convex Low-Rank Regularization for Image Compression Artifact Reduction. IEEE Transactions on Image Processing, 2020, 29, 5374-5385.	9.8	15
309	Soot formation and evolution in RP-3 kerosene inverse diffusion flames: Effects of flow rates and dimethyl carbonate additions. Fuel, 2020, 273, 117732.	6.4	15
310	Influence of water diversion system topologies and operation scenarios on the damping characteristics of hydropower units under ultra-low frequency oscillations. Energy, 2022, 239, 122679.	8.8	15
311	Density functional theory and reactive dynamics study of catalytic performance of TiO2 on CO2 desorption process with KHCO3/TiO2/Al2O3 sorbent. Molecular Catalysis, 2017, 439, 143-154.	2.0	14
312	On the effects of hydrogen addition in premixed formaldehyde flames. International Journal of Hydrogen Energy, 2017, 42, 3824-3832.	7.1	14
313	On the Response of Nascent Soot Nanostructure and Oxidative Reactivity to Photoflash Exposure. Energies, 2017, 10, 961.	3.1	14
314	SpyCatcher-N ^{TEV} : A Circularly Permuted, Disordered SpyCatcher Variant for Less Trace Ligation. Bioconjugate Chemistry, 2018, 29, 1622-1629.	3.6	14
315	On the treatment of self-absorption for temperature and concentration profiles reconstruction accuracy for soot and metal-oxide nanoparticles in nanofluid fuel flame using a CCD camera. Optik, 2018, 164, 114-125.	2.9	14
316	Combustion characteristics and synergy behaviors of biomass and coal blending in oxy-fuel conditions: A single particle co-combustion method. Science China Technological Sciences, 2018, 61, 1723-1731.	4.0	14
317	Checklist of oribatid mites (Acari, Oribatida) of the Russian Far East and Northeast of China. Zootaxa, 2018, 4472, 201.	0.5	14
318	EFFECTS OF NITRITE ANIONS ON SURFACE PASSIVE FILM PROPERTIES FOR Q235 CARBON STEELS. Surface Review and Letters, 2019, 26, 1850218.	1.1	14
319	Traffic surveillance video coding with libraries of vehicles and background. Journal of Visual Communication and Image Representation, 2019, 60, 426-440.	2.8	14
320	Accurate Parameter Estimation of a Hydro-Turbine Regulation System Using Adaptive Fuzzy Particle Swarm Optimization. Energies, 2019, 12, 3903.	3.1	14
321	Mesoporous Carbon and Ceria Nanoparticles Composite Modified Electrode for the Simultaneous Determination of Hydroquinone and Catechol. Nanomaterials, 2019, 9, 54.	4.1	14
322	The Curing Kinetics Analysis of Four Epoxy Resins Using a Diamine Terminated Polyether as Curing Agent. Thermochimica Acta, 2021, 702, 178987.	2.7	14
323	Morphology and Nanostructure Transitions of Soot with Various Dimethyl Ether Additions in Nonpremixed Ethylene Flames at Different Scales. Energy & Fuels, 2020, 34, 16705-16719.	5.1	14
324	Phase function effects on the retrieval of oceanic high-spectral-resolution lidar. Optics Express, 2019, 27, A654.	3.4	14

#	Article	IF	CITATIONS
325	Simultaneous reconstruction of temperature field and radiative properties by inverse radiation analysis using stochastic particle swarm optimization. Thermal Science, 2016, 20, 493-504.	1.1	14
326	Neuronal Population Reconstruction From Ultra-Scale Optical Microscopy Images via Progressive Learning. IEEE Transactions on Medical Imaging, 2020, 39, 4034-4046.	8.9	14
327	Operational characteristics and parameter sensitivity analysis of hydropower unit damping under ultra-low frequency oscillations. International Journal of Electrical Power and Energy Systems, 2022, 136, 107689.	5.5	14
328	Optimal design of hydro-wind-PV multi-energy complementary systems considering smooth power output. Sustainable Energy Technologies and Assessments, 2022, 50, 101832.	2.7	14
329	Improvement of Load-Following Capacity Based on the Flame Radiation Intensity Signal in a Power Plant. Energy & Fuels, 2008, 22, 1731-1738.	5.1	13
330	The genus <i>Notophthiracarus</i> of New Zealand (Acari: Oribatida: Phthiracaridae): three new species and a key to 24 described species. Zootaxa, 2013, 3682, 392-400.	0.5	13
331	Outage Analysis of Dual-Hop Transmission with Buffer Aided Amplify-and-Forward Relay. , 2014, , .		13
332	Field-widened Michelson interferometer for spectral discrimination in high-spectral-resolution lidar: practical development. Optics Express, 2016, 24, 7232.	3.4	13
333	Use of Debye's series to determine the optimal edge-effect terms for computing the extinction efficiencies of spheroids. Optics Express, 2017, 25, 20298.	3.4	13
334	Energy conversion and ignition of fluffy graphene by flash light. Energy, 2018, 144, 669-678.	8.8	13
335	Reconstruction model for temperature and concentration profiles of soot and metal-oxide nanoparticles in a nanofluid fuel flame by using a CCD camera. Chinese Physics B, 2018, 27, 054401.	1.4	13
336	Four-layer metallodielectric emitter for spectrally selective near-field radiative transfer in nano-gap thermophotovoltaics. Journal of Quantitative Spectroscopy and Radiative Transfer, 2018, 217, 235-242.	2.3	13
337	First-principles and experimental studies of [ZrO(OH)] ⁺ or ZrO(OH) ₂ for enhancing CO ₂ desorption kinetics – imperative for significant reduction of CO ₂ capture energy consumption. Journal of Materials Chemistry A, 2018, 6, 17671-17681.	10.3	13
338	Soot formation and combustion characteristics in confined mesoscale combustors under conventional and oxy-combustion conditions (O2/N2 and O2/CO2). Fuel, 2020, 264, 116808.	6.4	13
339	Spatiotemporal Generative Adversarial Network-Based Dynamic Texture Synthesis for Surveillance Video Coding. IEEE Transactions on Circuits and Systems for Video Technology, 2022, 32, 359-373.	8.3	13
340	Metal-organic framework assembly derived hierarchically ordered porous carbon for oxygen reduction in both alkaline and acidic media. Chemical Engineering Journal, 2022, 430, 132762.	12.7	13
341	SSSIC: Semantics-to-Signal Scalable Image Coding With Learned Structural Representations. IEEE Transactions on Image Processing, 2021, 30, 8939-8954.	9.8	13
342	An integrated modeling framework for cascading failure study and robustness assessment of cyber-coupled power grids. Reliability Engineering and System Safety, 2022, 226, 108654.	8.9	13

#	Article	IF	CITATIONS
343	Detailed influences of ethanol as fuel additive on combustion chemistry of premixed fuel-rich ethylene flames. Science China Technological Sciences, 2015, 58, 1696-1704.	4.0	12
344	Pattern recognition model for aerosol classification with atmospheric backscatter lidars: principles and simulations. Journal of Applied Remote Sensing, 2015, 9, 096006.	1.3	12
345	Combustion characteristics of nanofluid fuels in a half-opening slot tube. Science China Technological Sciences, 2017, 60, 1075-1087.	4.0	12
346	The geochronologic and geochemical constraints on the Early Cretaceous subduction magmatism in the central Lhasa subterrane, Tibet. Geological Journal, 2017, 52, 463-475.	1.3	12
347	Polarization properties of receiving telescopes in atmospheric remote sensing polarization lidars. Applied Optics, 2017, 56, 6837.	1.8	12
348	100 MW Peak Power Picosecond Laser Based on Hybrid End-Pumped Nd:YVO4 and Side-Pumped Nd:YAG Amplifiers. IEEE Journal of Selected Topics in Quantum Electronics, 2018, 24, 1-7.	2.9	12
349	The expression of natriuretic peptide receptors in developing zebrafish embryos. Gene Expression Patterns, 2018, 29, 65-71.	0.8	12
350	Compressed Image Restoration via Artifacts-Free PCA Basis Learning and Adaptive Sparse Modeling. IEEE Transactions on Image Processing, 2020, 29, 7399-7413.	9.8	12
351	Effects of aluminum addition on flash ignition and combustion of boron nanoparticles. Combustion and Flame, 2022, 236, 111762.	5.2	12
352	Boosting Li-CO2 battery performances by creating holey structure on CNT cathodes. Electrochimica Acta, 2022, 417, 140310.	5.2	12
353	In-situ construction of chemically bonded conductive polymeric network for high-performance silicon microparticle anodes in lithium-ion batteries. Journal of Power Sources, 2022, 539, 231591.	7.8	12
354	Preparation of optically active poly(N-propargylamide) gels and their application in chiral recognition. Macromolecular Research, 2011, 19, 729-733.	2.4	11
355	Poly(N-propargylamide)s bearing cholesteryl moieties: Preparation and optical activity. Reactive and Functional Polymers, 2012, 72, 832-838.	4.1	11
356	Redescription ofAustrotritia lebronneci(Oribotritiidae) and descriptions of two new species of Euphthiracaridae (Acari, Oribatida) from Australian Region. International Journal of Acarology, 2014, 40, 43-51.	0.7	11
357	Energy conversion and ignition of iron nanoparticles by flash. Science China Technological Sciences, 2017, 60, 1878-1884.	4.0	11
358	Effects of self-absorption on simultaneous estimation of temperature distribution and concentration fields of soot and metal-oxide nanoparticles in nanofluid fuel flames using a spectrometer. Journal of Quantitative Spectroscopy and Radiative Transfer, 2018, 212, 149-159.	2.3	11
359	Mechanism of core discing in the relaxation zone around an underground opening under high in situ stresses. Bulletin of Engineering Geology and the Environment, 2018, 77, 1179-1189.	3.5	11
360	Noncontact direct temperature and concentration profiles measurement of soot and metal-oxide nanoparticles in optically thin/thick nanofluid fuel flames. International Journal of Heat and Mass Transfer, 2019, 134, 237-249.	4.8	11

#	Article	IF	CITATIONS
361	A ribosomal DNA-hosted microRNA regulates zebrafish embryonic angiogenesis. Angiogenesis, 2019, 22, 211-221.	7.2	11
362	Character-Oriented Video Summarization With Visual and Textual Cues. IEEE Transactions on Multimedia, 2020, 22, 2684-2697.	7.2	11
363	A Semianalytic Monte Carlo Simulator for Spaceborne Oceanic Lidar: Framework and Preliminary Results. Remote Sensing, 2020, 12, 2820.	4.0	11
364	Utilization of carbon-based energy as raw material instead of fuel with low CO2 emissions: Energy analyses and process integration of chemical looping ammonia generation. Applied Energy, 2022, 312, 118809.	10.1	11
365	Six new species of the genus Euphthiracarus (Acari: Oribatida: Euphthiracaridae) from China. Zootaxa, 2012, 3481, 47.	0.5	10
366	Three new species of the genus Austrophthiracarus from New Zealand (Acari: Oribatida:) Tj ETQq0 0 0 rgBT /Over	rlock 10 Tf	50 542 Td (
367	Expression analysis of integrin β1 isoforms during zebrafish embryonic development. Gene Expression Patterns, 2014, 16, 86-92.	0.8	10
368	Generalized high-spectral-resolution lidar technique with a multimode laser for aerosol remote sensing. Optics Express, 2017, 25, 979.	3.4	10
369	Effects of auxiliary atmospheric state parameters on the aerosol optical properties retrieval errors of high-spectral-resolution lidar. Applied Optics, 2018, 57, 2627.	1.8	10
370	Zebrafish Embryo Vessel Segmentation Using a Novel Dual ResUNet Model. Computational Intelligence and Neuroscience, 2019, 2019, 1-14.	1.7	10
371	The effects of Bi ₂ O ₃ on the selective catalytic reduction of NO by propylene over Co ₃ O ₄ nanoplates. RSC Advances, 2019, 9, 32232-32239.	3.6	10
372	States, Trends, and Future of Aquaponics Research. Sustainability, 2020, 12, 7783.	3.2	10
373	Nanostructure and reactivity of soot from biofuel 2,5-dimethylfuran pyrolysis with CO2 additions. Frontiers in Energy, 2022, 16, 292-306.	2.3	10
374	Flow field characteristics, mixing and emissions performance of a lab-scale rich-quench-lean trapped-vortex combustor utilizing a quench orifice plate combined with a bluff-body. Chinese Journal of Aeronautics, 2021, 34, 476-492.	5.3	10
375	Deep Multi-Domain Prediction for 3D Video Coding. IEEE Transactions on Broadcasting, 2021, 67, 813-823.	3.2	10
376	Experimental and numerical study on sooting transition process in iso-octane counterflow diffusion flames: Diagnostics and combustion chemistry. Journal of the Energy Institute, 2021, 98, 282-293.	5.3	10
377	The somite-secreted factor Maeg promotes zebrafish embryonic angiogenesis. Oncotarget, 2016, 7, 77749-77763.	1.8	10

Reducing the NOx emissions during NH3 oxidation with Nickel modified Fe2O3-a promising378cost-effective and environmentally friendly catalyst for NH3 combustion. Combustion and Flame,5.2102022, 237, 111845.

#	Article	IF	CITATIONS
379	Intra Prediction via Edge-Based Inpainting. Proceedings of the Data Compression Conference, 2008, , .	0.0	9
380	New Zealand species of <i>Oribotritia</i> (Acari: Oribatida: Oribotritiidae): descriptions of two new species and a key to eight species. Systematic and Applied Acarology, 2013, 18, 153.	0.5	9
381	A Facile Method for Preparing Porous, Optically Active, Magnetic Fe ₃ O ₄ @poly(<i>N</i> â€acryloylâ€leucine) Inverse Core/Shell Composite Microspheres. Macromolecular Rapid Communications, 2014, 35, 91-96.	3.9	9
382	Antiviral Drug Ganciclovir Is a Potent Inhibitor of the Proliferation of Müller Glia–Derived Progenitors During Zebrafish Retinal Regeneration. , 2016, 57, 1991.		9
383	Review of the genus <i>Austrophthiracarus</i> (Acari, Oribatida, Phthiracaridae) with a description of a new species from Australia, a key to known species of the Australian Region and a world checklist. International Journal of Acarology, 2016, 42, 41-55.	0.7	9
384	Accelerated simulation of the degradation process of poly(arylene ether ketone)s containing alkylsulfonated side chains used as a proton exchange mmembrane. RSC Advances, 2017, 7, 8994-9001.	3.6	9
385	Understanding the mechanism of improvement in practical specific capacity using halogen substituted anthraquinones as cathode materials in lithium batteries. Electrochimica Acta, 2017, 224, 622-627.	5.2	9
386	Generation of a mef2aa:EGFP transgenic zebrafish line that expresses EGFP in muscle cells. Fish Physiology and Biochemistry, 2017, 43, 287-294.	2.3	9
387	Effects of carbon nanotubes additions on flash ignition characteristics of Fe and Al nanoparticles. Fullerenes Nanotubes and Carbon Nanostructures, 2018, 26, 168-174.	2.1	9
388	Failure Mechanism of Highly Stressed Rock Mass during Unloading Based on the Stress Arch Theory. International Journal of Geomechanics, 2018, 18, 04018146.	2.7	9
389	A molding method of Na2CO3/Al2O3 sorbents with high sphericity and low roughness for enhanced attrition resistance in CO2 sorption/desorption process via extrusion-spheronization method. Powder Technology, 2020, 366, 520-526.	4.2	9
390	Formation and characteristics of soot from pyrolysis of ethylene blended with furan fuels. Science China Technological Sciences, 2021, 64, 585-598.	4.0	9
391	New Zealand Austrophthiracarus (Acari: Oribatida: Phthiracaridae): three new species from North Island and offshore islands . Systematic and Applied Acarology, 2015, 20, 263.	0.5	9
392	Design of a high-spectral-resolution lidar for atmospheric temperature measurement down to the near ground. Applied Optics, 2019, 58, 9651.	1.8	9
393	Universal phase reconstruction approach of self-calibrating phase-shifting interferometry. Optics Letters, 2019, 44, 3857.	3.3	9
394	Chemical effects of carbon dioxide in ethylene, ethanol and DME counter-flow diffusion flames: An experimental reference for the fictitious CO2 flame. Journal of the Energy Institute, 2022, 100, 245-258.	5.3	9
395	Attribute Artifacts Removal for Geometry-Based Point Cloud Compression. IEEE Transactions on Image Processing, 2022, 31, 3399-3413.	9.8	9
396	Atropacarus(Atropacarus)niedbalaisp. nov., an extreme case of neotrichy in oribatid mites (Acari:) Tj ETQq0 0 0	rgBT /Ovei	lock 10 Tf 50

#	Article	IF	CITATIONS
397	Two new peculiar ptyctimous mites (Acari: Oribatida: Phthiracaridae) from the Australian region, with a key to 54 described species of <i>Notophthiracarus</i> â€Ramsay in Australia. Austral Entomology, 2014, 53, 159-166.	1.4	8
398	Descriptions of Two New Species of <i>Austrophthiracarus</i> Balogh et Mahunka, a Newly Recorded Genus of Ptyctimous Mites from China (Acari: Oribatida: Phthiracaridae). Annales Zoologici, 2014, 64, 267-272.	0.8	8
399	Review of Oribotritia (Acari, Oribatida, Oribotritiidae) with a world checklist and description of a new species from China . Zootaxa, 2015, 4007, 217.	0.5	8
400	Egfl6 is involved in zebrafish notochord development. Fish Physiology and Biochemistry, 2015, 41, 961-969.	2.3	8
401	Beam quality management by periodic reproduction of wavefront aberrations in end-pumped Nd:YVO_4 laser amplifiers. Optics Express, 2016, 24, 8988.	3.4	8
402	Mesoplophoroidea (Acari, Oribatida) of China. Zootaxa, 2016, 4084, 519-39.	0.5	8
403	Coupled chemical effects of carbon dioxide and hydrogen additions on premixed lean dimethyl ether flames. Science China Technological Sciences, 2017, 60, 102-115.	4.0	8
404	The Structure and Composition of Corrosion Product Film and its Relation to Corrosion Rate for Carbon Steels in CO2 Saturated Solutions at Different Temperatures. Journal of the Brazilian Chemical Society, 0, , .	0.6	8
405	Study on healing technique for weak interlayer and related mechanical properties based on microbially-induced calcium carbonate precipitation. PLoS ONE, 2018, 13, e0203834.	2.5	8
406	Robustness Assessment and Enhancement of Power Grids From a Complex Network's Perspective Using Decision Trees. IEEE Transactions on Circuits and Systems II: Express Briefs, 2019, 66, 833-837.	3.0	8
407	Expression analysis of the aquaporins during zebrafish embryonic development. Gene Expression Patterns, 2019, 32, 38-43.	0.8	8
408	Frank-Wolfe Network: An Interpretable Deep Structure for Non-Sparse Coding. IEEE Transactions on Circuits and Systems for Video Technology, 2020, 30, 3068-3080.	8.3	8
409	Water-Soluble Conductive Composite Binder for High-Performance Silicon Anode in Lithium-Ion Batteries. Batteries, 2022, 8, 54.	4.5	8
410	The Nature of Photocatalytic "Water Splitting―on Silicon Nanowires. Angewandte Chemie, 2015, 127, 3023-3028.	2.0	7
411	Hierarchical quadtree-based flexible block ordering in HEVC intra coding. , 2016, , .		7
412	Frequency locking of a field-widened Michelson interferometer based on optimal multi-harmonics heterodyning. Optics Letters, 2016, 41, 3916.	3.3	7
413	Flexible Nearâ€Infrared Photovoltaic Devices Based on Plasmonic Hotâ€Electron Injection into Silicon Nanowire Arrays. Angewandte Chemie, 2016, 128, 4653-4657.	2.0	7
414	Effects of hydrogen addition on nanostructure and reactivity of carbon particles in flame–wall interactions. Fullerenes Nanotubes and Carbon Nanostructures, 2018, 26, 756-764.	2.1	7

#	Article	IF	CITATIONS
415	Seedâ€5urface Grafting Precipitation Polymerization for Preparing Microsized Optically Active Helical Polymer Core/Shell Particles and Their Application in Enantioselective Crystallization. Macromolecular Rapid Communications, 2018, 39, e1800072.	3.9	7
416	Healing Technique for Rock Cracks Based on Microbiologically Induced Calcium Carbonate Mineralization. Journal of Materials in Civil Engineering, 2018, 30, .	2.9	7
417	Using Coal Coke for N-Sorption with an Al-based Nitrogen Carrier during Chemical Looping Ammonia Generation. Energy & Fuels, 2020, 34, 12527-12534.	5.1	7
418	Construction of Nighttime Cloud Layer Height and Classification of Cloud Types. Remote Sensing, 2020, 12, 668.	4.0	7
419	Formation and nanoscale-characteristics of soot from pyrolysis of ethylene blended with ethanol/dimethyl ether. Journal of the Energy Institute, 2020, 93, 1288-1304.	5.3	7
420	Fundamental Insights into Surface Modification of Silicon Material toward Improved Activity and Durability in Photocatalytic Hydrogen Production: A Case Study of Pre-Lithiation. Journal of Physical Chemistry C, 2021, 125, 5542-5548.	3.1	7
421	Revisiting seasonal dynamics of total nitrogen in reservoirs with a systematic framework for mining data from existing publications. Water Research, 2021, 201, 117380.	11.3	7
422	Instrument response effects on the retrieval of oceanic lidar. Applied Optics, 2020, 59, C21.	1.8	7
423	Review of Apoplophora (Acari: Oribatida: Mesoplophoridae), with the description of a new species from China. Zootaxa, 2009, 2051, 49-61.	0.5	6
424	<i>Microtritia</i> species from China (Acari: Oribatida: Euphthiracaridae), with description of a new species and a world key to species of the genus. International Journal of Acarology, 2014, 40, 402-409.	0.7	6
425	<p>Acrotritia species (Acari: Oribatida: Euphthiracaridae) from China with description of a new species</p> . Zootaxa, 2015, 3937, 127.	0.5	6
426	Inter-picture prediction based on 3D point cloud model. , 2015, , .		6
427	Three new species of the genus <i>Notophthiracarus</i> (Acari: Oribatida: Phthiracaridae), with an updated key to its known species in New Zealand. International Journal of Acarology, 2015, 41, 232-240.	0.7	6
428	Combining directional intra prediction and intra block copy with block partition for HEVC. , 2016, , .		6
429	Spatial distribution patterns of soil mite communities and their relationships with edaphic factors in a 30-year tillage cornfield in northeast China. PLoS ONE, 2018, 13, e0199093.	2.5	6
430	ICF target DT-layer refractive index and thickness from iterative analysis. Optics Express, 2018, 26, 17781.	3.4	6
431	Nanostructure and reactivity of nascent carbon particles from 2,5-dimethylfuran/n-heptane swirling inverse diffusion flames. Fullerenes Nanotubes and Carbon Nanostructures, 2019, 27, 106-119.	2.1	6
432	Synthesis of carbon nanotubes on metal mesh in inverse diffusion biofuel flames. Fullerenes Nanotubes and Carbon Nanostructures, 2019, 27, 77-86.	2.1	6

#	Article	IF	CITATIONS
433	Analysis of global three-dimensional aerosol structure with spectral radiance matching. Atmospheric Measurement Techniques, 2019, 12, 6541-6556.	3.1	6
434	Detrimental Effects and Prevention of Acidic Electrolytes on Oxygen Reduction Reaction Catalytic Performance of Heteroatom-Doped Graphene Catalysts. Frontiers in Materials, 2019, 6, .	2.4	6
435	Misalignment correction for free-form surface in non-null interferometric testing. Optics Communications, 2019, 437, 204-213.	2.1	6
436	Reference Clip for Inter Prediction in Video Coding. IEEE Transactions on Circuits and Systems for Video Technology, 2019, 29, 130-143.	8.3	6
437	Interferometric measurement of freeform surfaces using irregular subaperture stitching. Measurement Science and Technology, 2020, 31, 055202.	2.6	6
438	Performance Evaluation of Spaceborne Integrated Path Differential Absorption Lidar for Carbon Dioxide Detection at 1572 nm. Remote Sensing, 2020, 12, 2570.	4.0	6
439	E-Commerce Storytelling Recommendation Using Attentional Domain-Transfer Network and Adversarial Pre-Training. IEEE Transactions on Multimedia, 2022, 24, 506-518.	7.2	6
440	Electrocatalytic generation and tuning of ultra-stable and ultra-dense nanometre bubbles: an <i>in situ</i> molecular dynamics study. Nanoscale, 2021, 13, 11242-11249.	5.6	6
441	ls Heuristic Sampling Necessary in Training Deep Object Detectors?. IEEE Transactions on Image Processing, 2021, 30, 8454-8467.	9.8	6
442	Atropacarus (Hoplophorella) species (Acari: Oribatida: Phthiracaridae) from China, with descriptions of two new species. Systematic and Applied Acarology, 2014, 19, 166.	0.5	6
443	Species of Euphthiracarus (Acari: Oribatida: Euphthiracaridae) from China. Zootaxa, 2011, 2752, .	0.5	6
444	Efficient Dye Contaminant Elimination and Simultaneously Electricity Production via a Bi-Doped TiO2 Photocatalytic Fuel Cell. Nanomaterials, 2022, 12, 210.	4.1	6
445	Anemochore Seeds Harbor Distinct Fungal and Bacterial Abundance, Composition, and Functional Profiles. Journal of Fungi (Basel, Switzerland), 2022, 8, 89.	3.5	6
446	Meshed axisymmetric flame simulation and temperature reconstruction using light field camera. Optics and Lasers in Engineering, 2022, 158, 107159.	3.8	6
447	Critical role of connexin43 in zebrafish late primitive and definitive hematopoiesis. Fish Physiology and Biochemistry, 2010, 36, 945-951.	2.3	5
448	Descriptions of Two New Species of the Family Oribotritiidae (Acari: Oribatida: Euphthiracaroidea). Annales Zoologici, 2011, 61, 811-816.	0.8	5
449	НарруСо. , 2012, , .		5

450 Category-based dynamic recommendations adaptive to user interest drifts. , 2014, , .

#	Article	IF	CITATIONS
451	Three-Dimensional Point-Cloud Plus Patches: Towards Model-Based Image Coding in the Cloud. , 2015, , .		5
452	Two new species of the family Phthiracaridae (Acari, Oribatida) from New Zealand, including keys to all species ofPlonaphacarusandArphthicarusof the Australian region. International Journal of Acarology, 2015, 41, 584-589.	0.7	5
453	Design of the interferometric spectral discrimination filters for a three-wavelength high-spectral-resolution lidar. Optics Express, 2016, 24, 27622.	3.4	5
454	95-ps all-solid-state laser with a low-power microchip laser seed and a two-stage single-pass bounce geometry amplifier. Journal of the Optical Society of America B: Optical Physics, 2016, 33, 884.	2.1	5
455	Phthiracarusspecies (Acari: Oribatida: Phthiracaridae) from New Zealand, with description of a new species, redescription ofPhthiracarus pellucidusand a key to 19 described species from the Australian Region. Journal of Natural History, 2016, 50, 1463-1472.	0.5	5
456	Fatty Acid Binding Protein 11a Is Required for Brain Vessel Integrity in Zebrafish. Frontiers in Physiology, 2017, 8, 214.	2.8	5
457	Rotating a half-wave plate by 45°: An ideal calibration method for the gain ratio in polarization lidars. Optics Communications, 2018, 407, 361-366.	2.1	5
458	Facile Synthesis of FeS@C Particles Toward High-Performance Anodes for Lithium-Ion Batteries. Nanomaterials, 2019, 9, 1467.	4.1	5
459	Influence of self-absorption on reconstruction accuracy for temperature and concentration profiles of soot and metal-oxide nanoparticles in asymmetric nanofluid fuel flames. Optik, 2019, 178, 740-751.	2.9	5
460	Quadtree-Based Coding Framework for High-Density Camera Array-Based Light Field Image. IEEE Transactions on Circuits and Systems for Video Technology, 2020, 30, 2694-2708.	8.3	5
461	Detection of Chlorophyll a and CDOM Absorption Coefficient with a Dual-Wavelength Oceanic Lidar: Wavelength Optimization Method. Remote Sensing, 2020, 12, 3021.	4.0	5
462	Fault Diagnosis of Rotating Machinery Based on Convolutional Neural Network and Singular Value Decomposition. Shock and Vibration, 2020, 2020, 1-13.	0.6	5
463	Global pattern of studies on phosphorus at watershed scale. Environmental Science and Pollution Research, 2020, 27, 14872-14882.	5.3	5
464	Thermodynamic and economic analyses of a coal and biomass indirect coupling power generation system. Frontiers in Energy, 2020, 14, 590-606.	2.3	5
465	Systematic profiling of early regulators during tissue regeneration using zebrafish model. Wound Repair and Regeneration, 2021, 29, 189-195.	3.0	5
466	An efficient combination strategy for high-performance asymmetric-electrolyte metal–air batteries. Matter, 2021, 4, 1090-1092.	10.0	5
467	A review of Mesotritia (Acari: Oribatida: Oribotritiidae) in China, with descriptions of two new species and a checklist of known taxa. Zootaxa, 2010, 2479, 39.	0.5	5
468	Retrieving the microphysical properties of opaque liquid water clouds from CALIOP measurements. Optics Express, 2019, 27, 34126.	3.4	5

#	Article	IF	CITATIONS
469	Quantitative optical diagnostics on macroscopic soot onset for ethylene diffusion flames with ethyl ester addition. Optics Express, 2022, 30, 21410.	3.4	5
470	Three new species of the genus <i>Suctobelbella</i> (Acari: Oribatida: Suctobelbidae) from Sanjiang Plain, Northeast China. Zootaxa, 2013, 3637, 131-8.	0.5	4
471	 <p align="justify">Two new species of the genus Phrathicarus from New Zealand (Acari: Oribatida:) Tj ETQq1 1 0.784314 rgBT /C</p>)vælock 10) T f 50 657 1
472	First record of the genus <i>Arphthicarus</i> NiedbaÅ,a (Acari: Oribatida: Phthiracaridae) from China, with descriptions of two new species. Journal of Natural History, 2014, 48, 2199-2206.	0.5	4
473	Two new species of oribatid mites of the family Phthiracaridae (Acari, Oribatida) from Venezuela. International Journal of Acarology, 2014, 40, 443-448.	0.7	4
474	Two new species of <i>Austrophthiracarus</i> (Acari: Oribatida: Phthiracaridae) from Capleston Biological Reserve in New Zealand. International Journal of Acarology, 2016, 42, 416-419.	0.7	4
475	Fine-Grained Image Recognition from Click-Through Logs Using Deep Siamese Network. Lecture Notes in Computer Science, 2017, , 127-138.	1.3	4
476	Novel design of photoelectrochemical device by dual BiVO4 photoelectrode with abundant oxygen vacancy. Science Bulletin, 2018, 63, 1027-1028.	9.0	4
477	Synthesis of Amorphous Carbon Film in Ethanol Inverse Diffusion Flames. Nanomaterials, 2018, 8, 656.	4.1	4
478	Micro- and nano-structure evolution of soot from isooctane and 2,5-dimethylfuran flames in photocatalytic degradation. Fullerenes Nanotubes and Carbon Nanostructures, 2019, 27, 978-993.	2.1	4
479	Inverse radiation problem of multi-nanoparticles temperature and concentration fields reconstruction in nanofluid fuel flame. Optik, 2019, 181, 81-91.	2.9	4
480	Enhanced Corrosion Resistance and Photocatalytic Properties of Bi2O3/Phosphate Composite Film Prepared on AZ91D Magnesium Alloy by Phosphating. International Journal of Electrochemical Science, 2019, , 1434-1450.	1.3	4
481	Use of nanoparticles Cu/TiO(OH) ₂ for CO ₂ removal with K ₂ CO ₃ /KHCO ₃ based solution: enhanced thermal conductivity and reaction kinetics enhancing the CO ₂ sorption/desorption performance of K ₂ CO ₃ /KHCO ₃ 2019, 9, 10-18.		4
482	Treatment of efficiency for temperature and concentration profiles reconstruction of soot and metal-oxide nanoparticles in nanofluid fuel flames. International Journal of Heat and Mass Transfer, 2019, 133, 494-499.	4.8	4
483	Nanoscale inspection on carbon particles from commercial RP-3 kerosene combustion with different dilutions. Fullerenes Nanotubes and Carbon Nanostructures, 2020, 28, 959-972.	2.1	4
484	Effects of Magnetic Fields on Morphology and Nanostructure Evolution of Incipient Soot Particles from n-heptane/2,5-dimethylfuran Inverse Diffusion Flames. Journal of Thermal Science, 2020, 29, 820-839.	1.9	4
485	Tradeoff Between Robustness and Functionality in Cyber-Coupled Power Systems. IEEE Systems Journal, 2022, 16, 499-509.	4.6	4
486	Multiple scattering effects on the return spectrum of oceanic high-spectral-resolution lidar. Optics Express, 2019, 27, 30204.	3.4	4

#	Article	IF	CITATIONS
487	The Network Representation Learning Algorithm Based on Semi-Supervised Random Walk. IEEE Access, 2020, 8, 222956-222965.	4.2	4
488	Soil Rehabilitation Promotes Resilient Microbiome with Enriched Keystone Taxa than Agricultural Infestation in Barren Soils on the Loess Plateau. Biology, 2021, 10, 1261.	2.8	4
489	Characteristics of snowmelt transport in farmland soil in cold regions: The regulatory mechanism of biochar. Hydrological Processes, 2022, 36, .	2.6	4
490	Evolving framework of studies on global gulf ecosystems with Sustainable Development Goals. Environmental Science and Pollution Research, 2022, 29, 18385-18397.	5.3	4
491	Enhancing ionic conductivity in tablet–bottlebrush block copolymer electrolytes with well-aligned nanostructures <i>via</i> solvent vapor annealing. Journal of Materials Chemistry C, 2022, 10, 4247-4256.	5.5	4
492	Nonlinear Behavior and Reduced-Order Models of Islanded Microgrid. IEEE Transactions on Power Electronics, 2022, 37, 9212-9225.	7.9	4
493	Research on the Operational Strategy of the Hybrid Wind/PV/Small-Hydropower/Facility-Agriculture System Based on a Microgrid. Energies, 2022, 15, 2466.	3.1	4
494	Hopf Bifurcation and Parameter Sensitivity Analysis of a Doubly-Fed Variable-Speed Pumped Storage Unit. Energies, 2022, 15, 204.	3.1	4
495	Comprehensive optical diagnostics for flame behavior and soot emission response to a non-equilibrium plasma. Energy, 2022, 255, 124555.	8.8	4
496	Ultra-stretchable ion gels based on physically cross-linked polymer networks. Journal of Materials Chemistry C, 2022, 10, 10926-10934.	5.5	4
497	A new species ofSabahtritia(Acari: Oribatida: Synichotritiidae) from China. Oriental Insects, 2009, 43, 361-374.	0.3	3
498	Two new species of the genus <i>Notophthiracarus</i> (Acari: Oribatida: Phthiracaridae) from China. International Journal of Acarology, 2013, 39, 418-422.	0.7	3
499	Oribatid mites from Wanda Mountains in China, with description of a new species of the genus <i>Pilogalumna</i> . International Journal of Acarology, 2013, 39, 414-417.	0.7	3
500	Three new species of the genus Notophthiracarus from New Zealand (Acari:) Tj ETQq0 0	0 rgBT/Ov	erlogck 10 Tf 5
501	SIFT-preserving compression of mobile-captured license plate images for recognition. , 2014, , .		3
502	Co-occurrence patterns of above-ground and below-ground mite communities in farmland of Sanjiang Plain, Northeast China. Chinese Geographical Science, 2014, 24, 339-347.	3.0	3
503	<p align="left" class="Body">Review of the genus Acrotritia (Acari, Oribatida, Euphthiracaridae) with a world checklist, a key to known species of the Neotropical Region, and a description of a new species from Colombia</p> . Systematic and Applied Acarology, 2015, 20, 887.	0.5	3
504	Hoplophthiracarus species (Acari: Oribatida: Phthiracaridae) from China with descriptions of two new species. Biologia (Poland), 2015, 70, 1490-1494.	1.5	3

#	Article	IF	CITATIONS
505	Block the function of nonmuscle myosin II by blebbistatin induces zebrafish embryo cardia bifida. In Vitro Cellular and Developmental Biology - Animal, 2015, 51, 211-217.	1.5	3
506	New and little known ptyctimous mites (Acari: Oribatida) with a key to known species of Oribotritia from the Australasian Region. Biologia (Poland), 2016, 71, 917-923.	1.5	3
	⁢span style= ront-size: 10px; >New species of the family Steganacaridae (Acari, Oribatida,) IJ ETQq1 1 0.784	314 rgBT	Overlock]
507	style="font-size: 10px;">Austrophthiracarus and <em style="font-size: 10px;">Hoplophthiracarus	0.5	3
508	New Zealand Austrophthiracarus (Acari, Oribatida, Steganacaridae): two new species from the North Island. Zootaxa, 2018, 4500, 443.	0.5	3
509	Plonaphacarus species (Acari, Oribatida, Phthiracaridae) from China with descriptions of two new species and a key to Chinese species. Systematic and Applied Acarology, 2019, 24, 251.	0.5	3
510	Comparative study on soot characteristics of non-swirling and swirling inverse diffusion iso-octane flames with biofuel 2,5-dimethylfuran addition. Journal of the Energy Institute, 2020, 93, 2108-2123.	5.3	3
511	Comparative Study on Soot Reduction, Soot Nanostructure and Oxidation Reactivity of n-heptane/DMC and Isooctane/DMC Inverse Diffusion Flames. Journal of Thermal Science, 2020, 29, 1269-1281.	1.9	3
512	How soil texture, channel shape and crossâ€sectional area affect moisture dynamics and water loss in irrigation channels. Hydrological Processes, 2021, 35, e14155.	2.6	3
513	SIZ1 regulates phosphate deficiency-induced inhibition of primary root growth of Arabidopsis by modulating Fe accumulation and ROS production in its roots. Plant Signaling and Behavior, 2021, 16, 1946921.	2.4	3
514	On the treatment of lens optical center uncertainty in simultaneous reconstruction of flame temperature and soot volume fraction distributions by a CCD camera. Optik, 2021, 241, 167238.	2.9	3
515	Phthiracarus species from China with descriptions of three new speciesÂ(Acari:) Tj ETQq1 1	0.784314 0.5	1 ggBT /Ovel
516	Review of Austrotritia (Acari: Oribatida: Oribotritiidae), with descriptions of two new species from China. Zootaxa, 2009, 2144, 54-64.	0.5	3
517	纳米晶体在电å,¬åŒ–甲é,氧化å应ä,çš,,形貌æ•^应. Scientia Sinica Chimica, 2013, 43, 744-7	5 8. 4	3
518	Sub-5 nm homeotropically aligned columnar structures of hybrids constructed by porphyrin and oligo(dimethylsiloxane). Chemical Communications, 2021, 58, 108-111.	4.1	3
519	Ordered structure constructed from <i>C</i> ₂ -symmetric hexa- <i>peri</i> -hexabenzocoronene linked with oligo(dimethylsiloxane). Soft Matter, 2022, 18, 3430-3436.	2.7	3
520	Effects of Volumetric Property Models on the Efficiency of a Porous Volumetric Solar Receiver. Energies, 2022, 15, 3899.	3.1	3
521	Measurements and correlation of hydraulic resistance for H2O/CO2 mixtures at supercritical pressure. International Journal of Heat and Mass Transfer, 2022, 194, 123095.	4.8	3
522	Simulation study on radiative imaging of combustion flame in furnace. Journal of Zhejiang University: Science A, 2007, 8, 1853-1857.	2.4	2

#	Article	IF	CITATIONS
523	Improving Inverse Wavelet Transform by Compressive Sensing Decoding with Deconvolution. , 2009, , .		2
524	New Species of Oribatid Mites of the Families Parakalummidae and Galumnidae (Acari: Oribatida) from Xiao Hinggan Mountains, Northeastern China. Annales Zoologici, 2013, 63, 171-176.	0.8	2
525	Numerical Simulation of Advanced Small Pipe in Tunnels during Excavation by Steps. Applied Mechanics and Materials, 0, 353-356, 3699-3702.	0.2	2
526	Two new species of phthiracarid mites (Acari, Oribatida, Phthiracaridae) from Queensland, Australia. International Journal of Acarology, 2014, 40, 247-253.	0.7	2
527	Image semantic quality assessment for compression of car-plate images. , 2015, , .		2
528	Efficient background picture coding for videos obtained from static cameras. , 2015, , .		2
529	Effective Semisupervised Community Detection Using Negative Information. Mathematical Problems in Engineering, 2015, 2015, 1-8.	1.1	2
530	Highly sensitive lateral deformable optical MEMS displacement sensor: anomalous diffraction studied by rigorous coupled-wave analysis. Applied Optics, 2015, 54, 8935.	2.1	2
531	Two new species of the genus Mesotritia (Acari: Oribatida: Oribotritiidae) from China. International Journal of Acarology, 2018, 44, 395-399.	0.7	2
532	Hoplophthiracarus sidorchukae sp. nov. (Acari, Oribatida, Phthiracaridae) from the North Island, New Zealand. Zootaxa, 2019, 4647, 226-230.	0.5	2
533	Nanopore Sequencing and Hi-C Based De Novo Assembly of Trachidermus fasciatus Genome. Genes, 2021, 12, 692.	2.4	2
534	Taxonomic Study of the Genus <i>Maerkelotritia</i> Hammer, 1967 (Acari: Oribatida:) Tj ETQq0 0 0 rg	BT/Qverlo	ock 10 Tf 50
535	Water Cloud Detection with Circular Polarization Lidar: A Semianalytic Monte Carlo Simulation Approach. Sensors, 2022, 22, 1679.	3.8	2
536	Effects of diluent gases on sooting transition process in ethylene counterflow diffusion flames. RSC Advances, 2022, 12, 18181-18196.	3.6	2
537	Disparity-Aware Reference Frame Generation Network for Multiview Video Coding. IEEE Transactions on Image Processing, 2022, 31, 4515-4526.	9.8	2
538	Solar Energy Storage in an All-Vanadium Photoelectrochemical Cell: Structural Effect of Titania Nanocatalyst in Photoanode. Energies, 2022, 15, 4508.	3.1	2
539	Effects of flame temperature and radiation properties on infrared light field imaging. Case Studies in Thermal Engineering, 2022, 36, 102215.	5.7	2
540	Measurement of Three-Dimensional Temperature Distribution in an Absorbing, Emitting, and Anisotropically Scattering Medium. AIP Conference Proceedings, 2007, , .	0.4	1

#	Article	IF	CITATIONS
541	Manipulating image patches for compression. , 2008, , .		1
542	Soot Optical Properties in the Terahertz Spectra Domain. Journal of Heat Transfer, 2012, 134, .	2.1	1
543	Study on the Ground Settlement Regularity Caused by Deep Caving Method. Applied Mechanics and Materials, 0, 670-671, 907-911.	0.2	1
544	Image annotation via social diffusion analysis with common interests. , 2014, , .		1
545	Two new species of the genusEuphthiracarus(Acari: Oribatida: Euphthiracaridae) from Hainan Island, China. International Journal of Acarology, 2017, 43, 450-455.	0.7	1
546	On-line fall detection via a boosted cascade of hybrid features. , 2017, , .		1
547	Two new species of the genus Indotritia (Acari, Oribatida, Oribotritiidae) from China with a key to Chinese species. Systematic and Applied Acarology, 2018, 23, 1879.	0.5	1
548	Phthiracarus species (Acari, Oribatida, Phthiracaridae) from Northeast China with descriptions of two new species and a key to Chinese species. Systematic and Applied Acarology, 2018, 23, 1817.	0.5	1
549	Influences of NH 4 + ions and thin electrolyte layers (TEL) thickness on the corrosion behavior of AZ91D magnesium alloy. Materials and Corrosion - Werkstoffe Und Korrosion, 2019, 70, 2088-2102.	1.5	1
550	Effects of a nonideal half-wave plate on the gain ratio calibration measurements in polarization lidars. Applied Optics, 2017, 56, 8100.	1.8	1
551	<p class="Body">New findings of ptyctimous mites of the family Steganacaridae (Acari, Oribatida, Phthiracaroidea) from Yunnan Province, Southwest China</p> . Systematic and Applied Acarology, 2020, 25, 658-667.	0.5	1
552	Reflectance Reference for Intra-Frame Coding of Surveillance Video. Lecture Notes in Computer Science, 2018, , 481-491.	1.3	1
553	Semisupervised Community Preserving Network Embedding with Pairwise Constraints. Complexity, 2020, 2020, 1-14.	1.6	1
554	Detailed investigation of the iterative analysis for inertial confinement fusion target characterization. Applied Optics, 2020, 59, 10880.	1.8	1
555	Context-Adaptive Inverse Quantization for Inter-Frame Coding. IEEE Open Journal of Circuits and Systems, 2021, 2, 660-674.	1.9	1
556	Study of Cool Flames of Octane Isomers in the Counterflow Burner. Combustion Science and Technology, 0, , 1-15.	2.3	1
557	Photocatalytic Inactivation of Bacillus subtilis Spores by Natural Sphalerite with Persulfate under Visible Light Irradiation. Coatings, 2022, 12, 528.	2.6	1
558	Expression analysis of nel during zebrafish embryonic development. Gene Expression Patterns, 2022, 45, 119258.	0.8	1

#	Article	IF	CITATIONS
559	Vision-based tomographic reconstruction of emissivity distribution in asymmetric thermal plasma. Europhysics Letters, 2013, 103, 35002.	2.0	0
560	Research on the Stability of Surrounding Rock in Shallow Tunnel under Unsymmetrical Pressure Based on RDM. Applied Mechanics and Materials, 2013, 353-356, 1709-1712.	0.2	0
561	Research on Optimization of Excavating Seguence for Dawangou Tunnel. Applied Mechanics and Materials, 2013, 353-356, 3703-3706.	0.2	0
562	Study on Fluid-Structure Interaction Based on Hard Rock Deterioration Theory. Applied Mechanics and Materials, 0, 353-356, 1551-1554.	0.2	0
563	Visualization of user interests in online music services. , 2014, , .		0
564	Experimental study of inhibitor containing sulfur for mild steel in hydrochloric acid. Anti-Corrosion Methods and Materials, 2016, 63, 275-280.	1.5	0
565	Contribution to the knowledge of the oribatid mite genus Mesoplophora (Acari: Oribatida:) Tj ETQq1 1 0.784314 1215-1221.	rgBT /Ove 1.5	erlock 10 Té O
566	Reply to Comments by Jia Yue on "Global Distribution and Variations of NO Infrared Radiative Flux and Its Responses to Solar Activity and Geomagnetic Activity in the Thermosphere― Journal of Geophysical Research: Space Physics, 2018, 123, 10,419.	2.4	0
567	<p class="Body">Contribution to the knowledge of the oribatid mite genus Apoplophora (Acari, Oribatida, Apoplophoridae) with description of a new species from China</p> . Systematic and Applied Acarology, 2019, 24, 1911-1917.	0.5	0
568	Contribution to the knowledge of the ptyctimous mite genus Austrophthiracarus (Acari, Oribatida, Steganacaridae) with descriptions of two new species from China . Zootaxa, 2020, 4786, 138-144.	0.5	0
569	New species of the subgenus <i>Hoplophorella</i> (Oribatida: Steganacaridae: <i>Atropacarus</i>) from South China. International Journal of Acarology, 2021, 47, 89-94.	0.7	0
570	Three Dimensional Simulation of Electrical Impedance Tomography for Imaging Vocal Folds Within the Human Neck. Journal of Medical Imaging and Health Informatics, 2017, 7, 1509-1516.	0.3	0
571	A pressure-tuned field-widened Michelson interferometer system as the spectroscopic filter of high-spectral-resolution lidar. , 2018, , .		0
572	Structure of Macrobenthic Assemblages and Its Relationship with Environmental Variables in the East China Sea of Xiangshan. Pakistan Journal of Zoology, 2018, 51, .	0.2	0
573	Arphthicarus olszanowskii sp. nov. (Acari: Oribatida: Steganacaridae) from Tibet, China with a Key to Known Species of Arphthicarus from the Palaearctic and Oriental Regions. Annales Zoologici, 2020, 70, .	0.8	0
574	Lidar Ratio Regional Transfer Method for Extinction Coefficient Accuracy Improvement in Lidar Networks. Remote Sensing, 2022, 14, 626.	4.0	0
575	MicroRNA-22 coordinates vascular and motor neuronal pathfinding via <i>sema4</i> during zebrafish development. Open Biology, 2022, 12, 210315.	3.6	0
576	Probing sooting limits in counterflow diffusion flames via multiple optical diagnostic techniques. Experimental Thermal and Fluid Science, 2022, 136, 110679.	2.7	0